4-23-2020

Electromagnetically Induced Transparency and the Polarization of Laser Light

John LaPonte
Lake Forest College, laponte j@lakeforest.edu

Electromagnetically Induced Transparency and the Polarization of Laser Light

Abstract

This thesis investigates the phenomenon of electromagnetically induced transparency (EIT). This experiment uses a 790 nm diode laser to drive transitions in rubidium atoms. The D1 line of Rubidium was used, which involves the transitions from the $5S_{1/2}$ and $5P_{1/2}$ hyperfine states. This experiment investigates the effect of the quality of polarization on EIT. Careful techniques were used to improve the quality of the polarization of the laser light.

Document Type

Thesis

Degree Name

Bachelor of Arts (BA)

Department or Program

Physics

First Advisor

Michael M. Kash

Second Advisor

Nathan Mueggenburg

Third Advisor

Arthur Bousquet

Subject Categories

Atomic, Molecular and Optical Physics

LAKE FOREST COLLEGE

Senior Thesis

Electromagnetically Induced Transparency and the Polarization of Laser Light

by

John LaPonte

April 23, 2020

The report of the investigation undertaken as a
Senior Thesis, to carry two courses of credit in
the Department of Physics

_____	_____
Davis Schneiderman	Michael M. Kash, Chairperson
Krebs Provost and Dean of the Faculty	
	_____
	Nathan Mueggenburg
	_____
	Arthur Bousquet

ABSTRACT

This thesis investigates the phenomenon of electromagnetically induced transparency (EIT). This experiment uses a 790 nm diode laser to drive transitions in rubidium atoms. The D1 line of Rubidium was used, which involves the transitions from the $5S_{1/2}$ and $5P_{1/2}$ hyperfine states. This experiment investigates the effect of the quality of polarization on EIT. Careful techniques were used to improve the quality of the polarization of the laser light.

ACKNOWLEDGMENTS

I want to thank Dr. Kash and Dr. Mueggenburg for being amazing professors. I would not have had such an amazing experience at Lake Forest College without them. Both Dr. Kash and Dr. Mueggenburg were always available to help with homework or anything else I needed help with. I had a great time working with both of them over the summer and taking as many classes with them as I could. They each have the ability to make challenging material exciting to learn. I want to thank both of them for going above and beyond as great professors, mentors, and friends.

I also want to thank my parents and the rest of my family for always supporting my decisions. I would not have been able to get through school and football without everything my parents did for me. I knew I did not have to worry about making mistakes my four years at Lake Forest College because my family would always have my back.

Lastly I want to thank the football program. Hanging with my teammates allowed me to balance hard work and having a good time in college. I want to thank my coaches for supporting me and making the balance between school and sports easy to manage.

I want to thank all of the other people that have helped and supported me throughout my years at Lake Forest College. Without my family and friends I would not have been able to have a successful four years of college.

TABLE OF CONTENTS

I. Introduction

Electromagnetically Induced Transparency (EIT) occurs when a medium that should absorb light does not. In this experiment, a cell containing rubidium vapor prepared by a beam of light with particular characteristics is the medium. When the second beam of light is applied, light that was absorbed is now transmitted through the medium.

Physicists have recently employed EIT to demonstrate different phenomena. Laser action without population inversion, high sensitivity to magnetic fields, and slowing pulses of light are examples of these different phenomena. The end goal of this project was to improve EIT by improving the quality of the light beams.

The character of light beams focused on here is *polarization.* Polarization is the direction of the electric field vector in a classical electromagnetic wave. This project will focus on improving the quality of the linear and circular polarization of the laser beam.

I will start with discussing fundamental theories for atoms and light waves. I will review the structure of the splitting of energy levels in hydrogen and rubidium atoms. The splitting in energy levels lead to the absorption and transmission of photons in the atoms. Next I will discuss the experimental apparatus and equipment used in this project. Finally I will present data gathered for the polarization of the light beams and EIT.

II. Theory

To explain the theory behind electromagnetically induced transparency (EIT), I will first need to review more fundamental theories. I will start with the hydrogen atom as a simple model that is similar to rubidium. I will look at the energy levels in hydrogen and the fine and hyperfine splitting of these energy levels. Then, I will look at the rubidium atom. I will relate rubidium to hydrogen to establish the fine and hyperfine splitting of the energy levels in rubidium. Next, I will discuss the polarization of light and look more specifically into linear and circular polarization. Finally, I will describe the phenomenon of EIT. The energy levels of rubidium and the polarization of light are needed to develop the theory of EIT.

A. Hydrogen Atom

The hydrogen atom is the simplest atom to study. The basic model of the hydrogen atom is the Bohr Model. The Bohr model describes the hydrogen atom as a motionless nucleus with an orbiting electron. The nucleus is composed of a proton with positive charge *e*, and the electron has charge –*e*. The structure of the hydrogen atom is important in this experiment because rubidium has a similar structure. The energy levels of the hydrogen atom serve as a more simplistic version of the energy levels of rubidium.

1. Energy levels

$$i\hbar\frac{\partial\Psi}{\partial t} = -\frac{\hbar^2}{2m}\nabla^2\Psi + V\Psi \tag{1}$$

This is the Schrödinger equation,[1] which is used to solve for the wave

function, $\Psi(x,t)$. Here $\hbar$ is Planck's constant divided by 2π, i is the square root of -1, *m* is the mass, and V is the potential energy function. For the hydrogen atom, the potential energy function comes from Coulomb's Law,

$$V(r) = -\frac{e^2}{4\pi\epsilon_0}\frac{1}{r} \tag{2}$$

where r is the separation between the nucleus and the electron and ϵ_0 is the permittivity of free space. The Schrödinger equation combined with this potential is used to solve for the energy levels of the hydrogen atom. Solving the Schrödinger equation for the energy of a hydrogen atom reveals only certain energy levels are allowed and are numbered by n , the principle quantum number. The allowed energies are[2]

$$E_n = -\left[\frac{m_e}{2\hbar^2}\left(\frac{e^2}{4\pi\epsilon_0}\right)^2\right]\frac{1}{n^2} = \frac{E_1}{n^2} \quad \text{where} \quad n = 1, 2, 3... \tag{3}$$

$$\text{and, } E_1 = -\left[\frac{m_e}{2\hbar^2}\left(\frac{e^2}{4\pi\epsilon_0}\right)^2\right] = -13.6\text{eV} \tag{4}$$

These energy levels are important because they determine the absorption and emission of the hydrogen atom. The electron can be excited into higher energy levels and transition back to lower energy levels. These are called quantum jumps, and when electrons jump to a lower energy level they give off photons, and they can absorb photons to move up in energy levels. When making these quantum jumps, the hydrogen atom can still only be in the allowed energy states, this enables calculations for the energy of the photons.

$$E_\gamma = E_i - E_f = -13.6\text{eV}\left(\frac{1}{n_i^2} - \frac{1}{n_f^2}\right) \tag{5}$$

Then, combining the Planck formula

$$E_\gamma = h\upsilon = \frac{hc}{\lambda} \tag{6}$$

with the difference of energies leads to the Rydberg formula[3]

$$\frac{1}{\lambda} = R\left(\frac{1}{n_f^2} - \frac{1}{n_i^2}\right) \quad \text{where,} \quad R \equiv \frac{m_e}{4\pi c\hbar^3}\left(\frac{e^2}{4\pi\text{Ú}_0}\right)^2 \tag{7}$$

where R is the Rydberg constant. Now, the specific wavelength of photons that can be emitted from or absorbed into a hydrogen atom can be calculated.

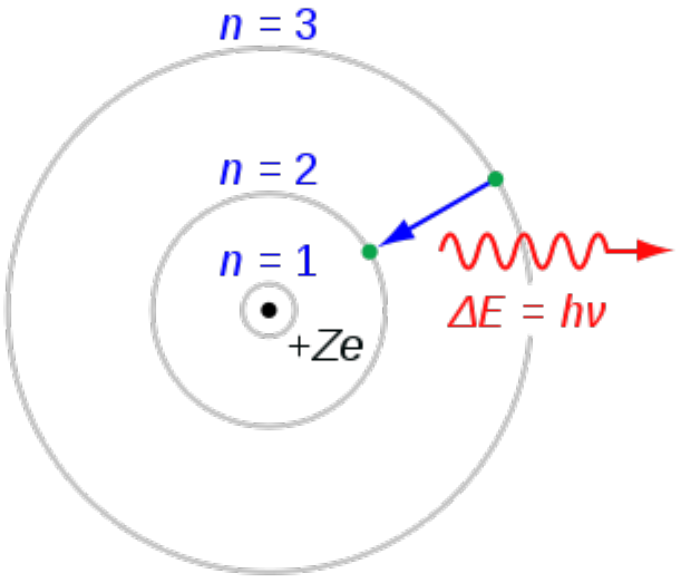

FIG. 1.[4] The Bohr model of the hydrogen atom (for hydrogen Z=1). In this figure the electron is transitioning down from the n=3 energy level to the n=2 energy level. The wavelength of the emitted photon can be calculated using the Rydberg formula

2. Fine Structure of Hydrogen

The Schrödinger equation can be used for hydrogen to solve for the different energy levels, however there are still corrections to be made to improve accuracy of calculations. One simple correction to account for the motion of the nucleus is replacing the mass m with the reduced mass μ. This correction raises the energy levels in hydrogen. Another correction that shifts the energy levels is called the Lamb Shift. A more important correction for this experiment is known as the fine structure of hydrogen. Time-independent first-order perturbation theory is needed to solve for the fine structure correction. The fine structure correction lowers the energy levels and splits some of the energy levels. This correction can be broken into two separate components: spin-orbit coupling, and a relativistic correction. These separate components are caused by different effects but are grouped together because they have a similar magnitude. The relativistic correction is needed to account for the relativistic speed that the electron travels. For the relativistic correction, the relativistic momentum is used to express the kinetic energy. This creates a new perturbation Hamiltonian where the first-order correction is [5]

$$H_r^{'} = -\frac{p^4}{8m_e{}^3c^2} \tag{8}$$

and taking the expectation value of the Hamiltonian yields the first-order energy correction,[6]

$$E_r^1 = \left\langle H_r^{'} \right\rangle = -\frac{\left(E_n\right)^2}{2m_e c^2}\left[\frac{4n}{\ell + 1/2} - 3\right] \tag{9}$$

where E_n is the Bohr energy and ℓ is the orbital angular momentum quantum number. The relativistic correction shifts the energies below the Bohr energies.

Spin-orbit coupling is due to the proton's motion in the electron's frame of reference. The proton orbits around the electron creating a magnetic field that exerts a torque on the magnetic dipole moment of the spinning electron. This creates the perturbed Hamiltonian,[7]

$$H'_{\text{so}} = \left(\frac{e^2}{8\pi\varepsilon_0} \right) \frac{1}{m_e^2 c^2 r^3} \mathbf{S} \cdot \mathbf{L} \tag{10}$$

where $\mathbf{S}$ and $\mathbf{L}$ are the spin angular momentum vector and the orbital angular momentum vector. Taking the expectation value of the perturbed Hamiltonian yields the first-order energy correction called the spin-orbit correction energy,

$$E^1_{\text{so}} = \left\langle H'_{\text{so}} \right\rangle = \frac{(E_n)^2}{m_e c^2} \left\{ \frac{n\left[j(j+1) - \ell(\ell+1) - 3/4 \right]}{\ell(\ell+1/2)(\ell+1)} \right\} \tag{11}$$

where j is the total electronic angular momentum quantum number. Combining the relativistic energy correction with the spin-orbit correction gives the complete fine structure formula.

$$E^1_{\text{fs}} = \frac{(E_n)^2}{2m_e c^2} \left(3 - \frac{4n}{j+1/2} \right) \tag{12}$$

Then, combining this with the Bohr formula gives the energy levels of hydrogen including the first-order fine structure correction.

$$E_{nj} = -\frac{13.6\text{eV}}{n^2} \left[1 + \frac{\alpha^2}{n^2} \left(\frac{n}{j+1/2} - \frac{3}{4} \right) \right] \quad \text{where} \quad \alpha = \frac{e^2}{4\pi\varepsilon_0 \hbar c} \tag{13}$$

Here α is the fine structure constant. The fine structure correction breaks down the Bohr energies and gives us slightly different energies for different values of ℓ. The fine structure correction is a factor of α^2 smaller than the Bohr energies.

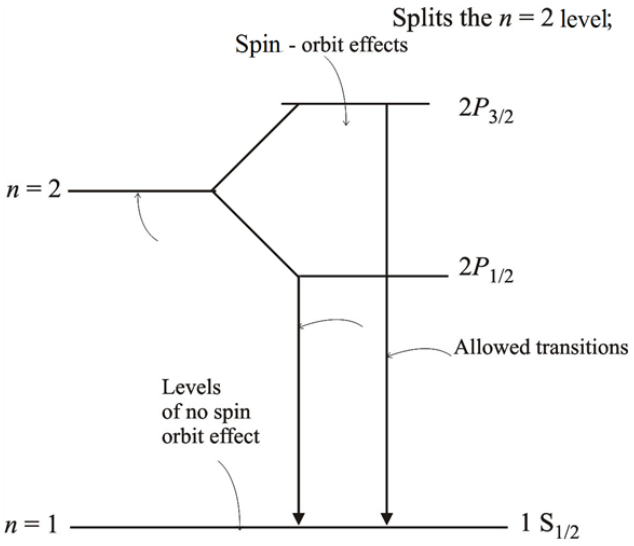

FIG. 2.[8] The splitting of the n=2 energy level of hydrogen due to the spin-orbit coupling. The actual energy levels would be lower than the Bohr energies due to the relativistic correction.[9]

3. Hyperfine Structure of Hydrogen

The hyperfine structure of hydrogen is caused by the effect of the proton's magnetic dipole moment on the electron. The magnetic dipole moment of a proton $\boldsymbol{\mu}_{\mathbf{p}}$ creates a magnetic field.[10]

$$\boldsymbol{\mu}_{\mathbf{p}} = \frac{g_p e}{2m_p}\mathbf{S}_{\mathbf{p}} \qquad \mathbf{B} = \frac{\mu_0}{4\pi r^3}\left[3\left(\boldsymbol{\mu}_{\mathbf{p}}\cdot\hat{r}\right)\hat{r} - \boldsymbol{\mu}_{\mathbf{p}}\right] + \frac{2\mu_0}{3}\boldsymbol{\mu}_{\mathbf{p}}\delta^3(\mathbf{r}) \tag{14}$$

Where g_p is the gyromagnetic ratio for a proton, m_p is the mass of a proton, $\mathbf{S}_{\mathbf{p}}$ is the angular momentum vector for the proton, μ_0 is the permeability of free space, and

$\delta^3(\mathbf{r})$ is the Dirac delta function. Then the perturbed Hamiltonian of the electron in the magnetic field created by the proton's magnetic dipole moment is

$$H'_{\text{hf}} = \frac{\mu_0 g_p e^2}{8\pi m_p m_e} \frac{\left[3\left(\mathbf{S_p}\cdot\hat{r}\right)\left(\mathbf{S_e}\cdot\hat{r}\right) - \mathbf{S_p}\cdot\mathbf{S_e}\right]}{r^3} + \frac{\mu_0 g_p e^2}{3m_p m_e}\mathbf{S_p}\cdot\mathbf{S_e}\delta^3(\mathbf{r}) \tag{15}$$

Calculating the expectation of the Hamiltonian gives the first-order correction to the energy

$$E^1_{\text{hf}} = \frac{\mu_0 g_p e^2}{3\pi m_p m_e a^3}\left\langle \mathbf{S_p}\cdot\mathbf{S_e}\right\rangle \quad \text{where} \quad a = \frac{4\pi\acute{U}_0\hbar^2}{m_e e^2} \tag{16}$$

where a is the Bohr radius. This is called spin-spin coupling because of the dot product of the two spins. Taking the dot product of the spins of the electron and proton either results in a total spin of 1 or 0. The spin of 1 yields a triplet state and the spin of 0 yields a singlet state. The energy gap between the triplet and singlet states is defined as

$$\Delta E = \frac{4 g_p \hbar^4}{3 m_p m_e^2 c^2 a^4} = 5.88\times10^{-6}\,\text{eV} \tag{17}$$

This correction is a factor of $\left(\frac{m_e}{m_p}\right)\alpha^2$ smaller than the Bohr energy. This is about 1800 times smaller than the fine structure correction because the mass of the proton is much larger than the mass of the electron.

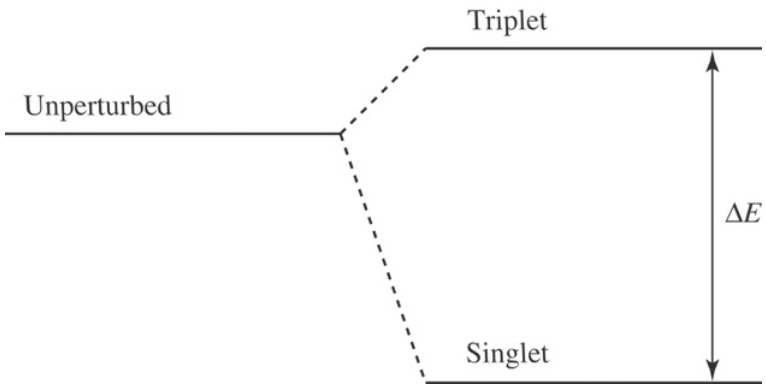

FIG. 3.[11] Splitting of the hyperfine structure of the ground state of hydrogen. The unperturbed state is split into a singlet and triplet state after the first order correction

B. Rubidium

Rubidium is an alkali metal with an atomic number of 37. Rubidium possesses many qualities that are useful for this experiment. The ground state configuration of the electrons in rubidium is

$$(1s)^2(2s)^2(2p)^6(3s)^2(3p)^6(4s)^2(3d)^{10}(4p)^6(5s)^1 \tag{18}$$

The first 36 electrons are stable leaving one valence electron in the 5s orbital. The outer most electron in the 5s orbital has an angular momentum quantum number of $L=0$, and when excited the electron moves into the 5p orbital with $L=1$. The transitions to and from the 5s and 5p orbitals will be used in this experiment. Rubidium's one valence electron makes rubidium hydrogenic, meaning "like hydrogen", this is one of many useful properties of rubidium. Another useful property of Rubidium is it easily vaporizes at relatively low temperatures. In this lab, cell heaters were used to vaporize the rubidium atoms in the cell. Rubidium being hydrogenic means rubidium

acts similarly to hydrogen and we can expect the fine and hyperfine structure of rubidium to be very similar to that of hydrogen. In this experiment ^{87}Rb and ^{85}Rb are the two rubidium isotopes used. ^{85}Rb is the only stable isotope of rubidium, but ^{87}Rb decays slowly enough to be treated as stable.[12] Both isotopes of Rubidium are used in the reference cell, but only ^{87}Rb is used in the interaction cell.

1. Fine Structure of Rubidium

The fine structure of rubidium is similar to that of hydrogen, but it is much more complicated. Like in hydrogen, the fine structure correction is due to the relativistic correction combined with the spin-orbit coupling. The relativistic correction shifts the energy levels below the Bohr energies, and the spin-orbit coupling splits the energy levels. To define the state of the atom the notation used is[13]

$$n^{2S+1}L_J \tag{19}$$

The relativistic correction shifts the 5^2S orbital into the $5^2S_{1/2}$ sublevel. The relativistic correction shifts the 5^2P orbital down and the spin-orbit coupling splits it into the $5^2P_{1/2}$ and $5^2P_{3/2}$ sublevels. The transition from the $5^2P_{1/2}$ state to the $5^2S_{1/2}$ state is called the D1 line. The transition from the $5^2P_{3/2}$ state to the $5^2S_{1/2}$ state is called the D2 line.[14] The D1 line is used in this experiment because it involves fewer states and is easier to work with. The D1 line corresponds to photons emitted and absorbed at a wavelength of approximately 795 nm, which is the wavelength of our laser. The D2 line corresponds to a smaller wavelength of about 780 nm.[15]

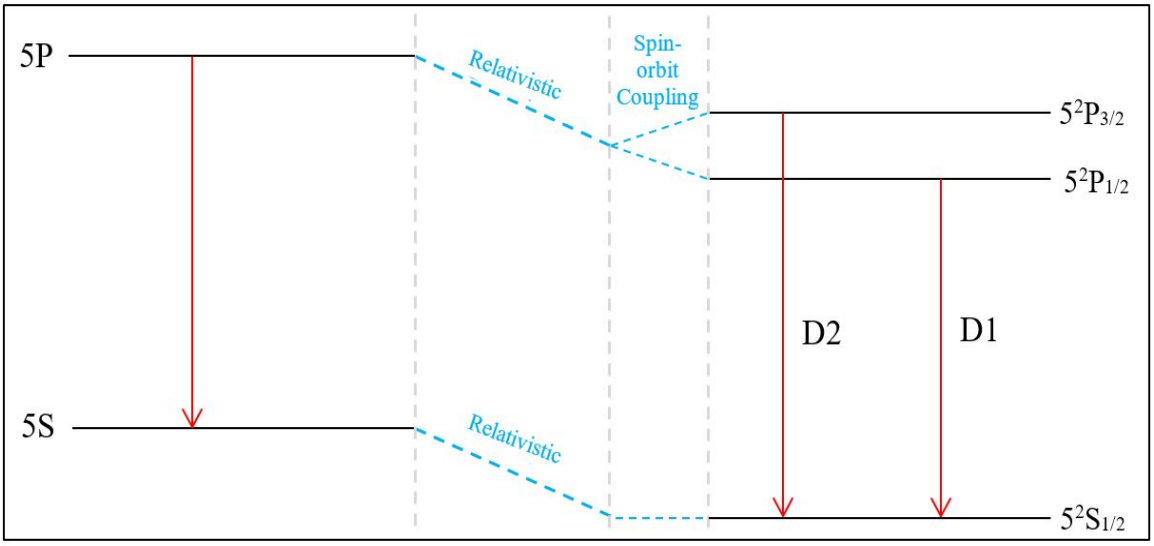

FIG. 4.[16] The fine structure splitting of states in rubidium. The states are shifted down because of the relativistic correction. The 5P orbital is split due to the spin-orbit coupling.

2. Hyperfine Structure of Rubidium

The hyperfine structure of Rubidium is caused by the interaction of the magnetic dipole moments of the nucleus and electron. The hyperfine structure causes the split states due to the fine structure splitting to be split again. The hyperfine splitting for each state depends on the total angular momentum quantum number F[17]

$$\mathbf{F} = \mathbf{J} + \mathbf{I} \tag{20}$$

Where $\mathbf{J}$ is the total electronic angular momentum, and $\mathbf{I}$ is the total nuclear angular momentum. By the rules of adding angular momentum, F ranges from,

$$|J - I| \leq F \leq J + I \tag{21}$$

in integer steps. For ^{87}Rb $I = 3/2$[18], and in the D1 line the $5^2S_{1/2}$ and the $5^2P_{1/2}$ states

each have $J = 1/2$. Therefore, the total angular momentum quantum number can be 1 or 2 for each state. The two different values for F split the fine structure states into two different hyperfine structure states.

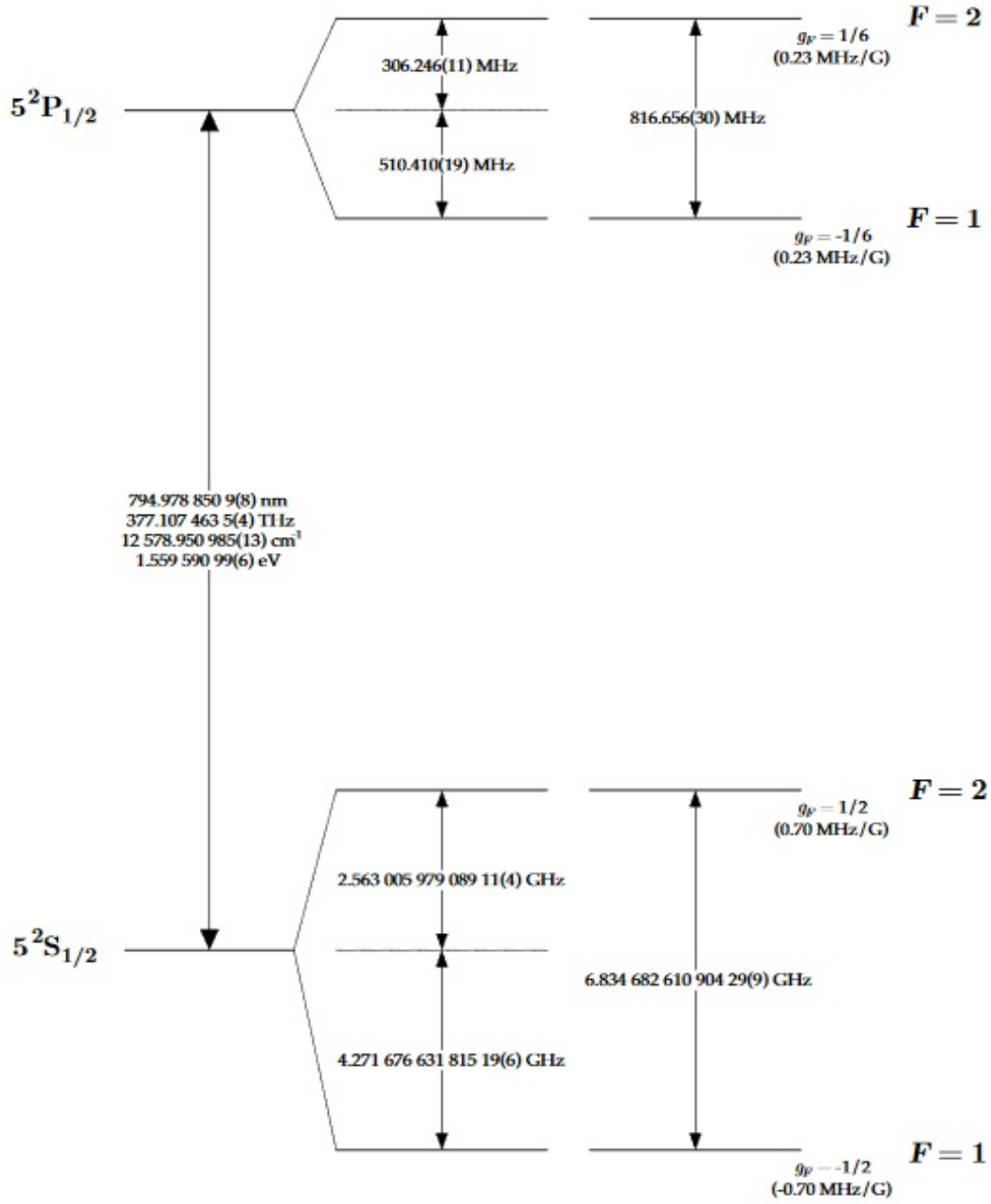

FIG. 5.[19] The hyperfine splitting of the D1 line in ^{87}Rb. The two fine structure states are split into their different values of F. This diagram includes wavelengths, frequencies, F values, energies, and g-factors.

After the splitting, the D1 line now has 4 different available transitions. The first and smallest transition labeled c is from the transition from $F=2$ for the $5^2S_{1/2}$ state to $F=1$ for the $5^2P_{1/2}$ state. The second transition labeled d is from the $F=2$ for the $5^2S_{1/2}$ state to the $F=2$ for the $5^2P_{1/2}$ state. The third transition e is from the $F=1$ for the $5^2S_{1/2}$ state to the $F=1$ for the $5^2P_{1/2}$ state. The final transition f id from the $F=1$ for the $5^2S_{1/2}$ state to the $F=2$ for the $5^2S_{1/2}$ state.

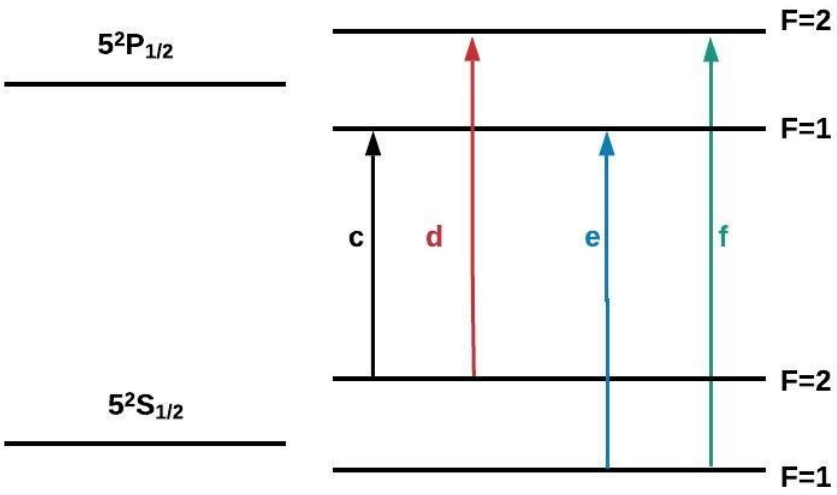

FIG. 6. The four transitions of the D1 line in rubidium. The $5^2P_{1/2}$ and $5^2S_{1/2}$ are split due to the hyperfine structure of rubidium. The four different energy levels allow for four separate transitions. The labels for the transitions come from an American Journal of Physics article.[20]

The hyperfine levels break down further into magnetic sublevels. The sublevels are labeled based on the magnetic quantum number m_f. The values of the magnetic quantum number range from,

$$-F \le m_f \le F \tag{22}$$

in integer steps. Therefore, for $F = 1$, m_f can be -1, 0, or 1, and for $F = 2$, m_f can be -2, -1, 0, 1, or 2. Due to the Zeeman Effect, the different magnetic sublevels have slightly different energies when an external magnetic field is applied. When there is no external magnetic field the magnetic sublevels are degenerate for the same value of F. The transitions between these magnetic sublevels depends on quantum mechanics selection rules[21]

$$\Delta m_f = 0 \text{ or } \pm 1 \tag{23}$$

In this experiment the change in m_f is known based on what kind of light excites the atom. If the atom is excited by right circularly polarized light, then m_f decreases by a value of 1. If the atom is excited by left circularly polarized light, then m_f increases by a value of 1. This sublevels and selection rules will be important to achieve EIT in rubidium.

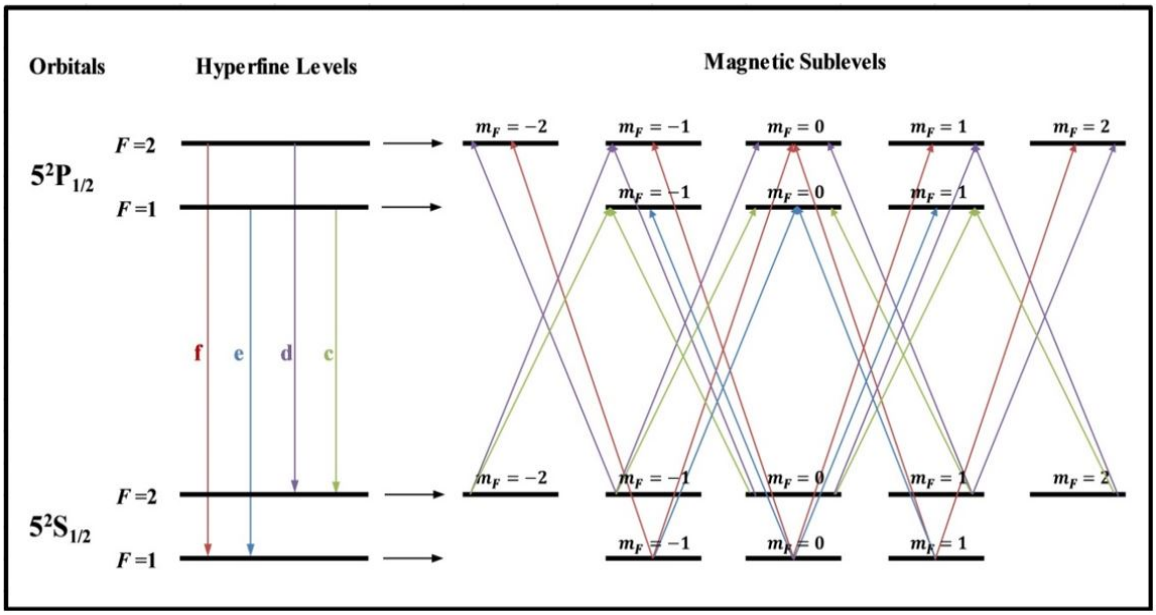

FIG. 7.[22] Hyperfine levels split into magnetic sublevels. The figure shows the magnetic sublevels if no external magnetic field is applied so the sublevels are degenerate for the same value of F. The transitions shown are the allowed transitions in the D1 line of Rubidium according to the selection rules. The different transitions for different F values are labeled and color coded.

C. Polarization

Light is an electromagnetic wave that can be classified as a transverse wave. If a light wave is propagating in a direction, the electric and magnetic fields in the wave oscillate perpendicular to each other and the direction of propagation. Polarization is defined as the description of the vibration of the electric field in a light wave[23]. There is a wide array of different types of polarizations, with linear polarization at one end, and circular polarization at the other.

Light is said to be linearly polarized when the vibration is along one direction. Light can be linearly polarized in any orientation perpendicular to the propagation of the light. Commonly, the terms vertical linear polarization and horizontal linear polarization

are used. Vertical linear polarization refers to polarization perpendicular to the surface of the lab table, horizontal linear polarization refers to polarization parallel to the surface of the lab table. Much different than linear polarization, there is circular polarization. Light is circularly polarized when the direction of polarization rotates about the direction of propagation. Circular polarization can be split up into two simple categories of right and left circularly polarized light. Light is right circularly polarized when the electric field rotates in the clockwise direction when looking at the source, and is left circularly polarized when it rotates in the counter clockwise direction.

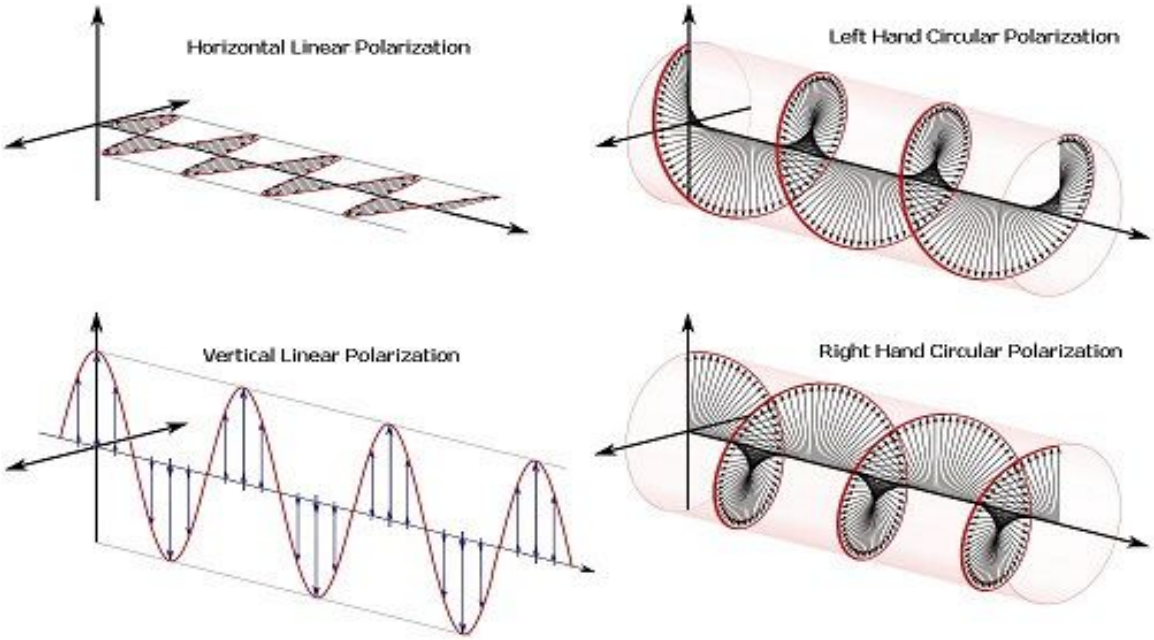

FIG. 8.[24]Linear and circular polarization. On the left there is linearly polarized light. The direction and magni1tude of the arrows represent the electric field of the light. On the right the diagrams show circularly polarized light.

D. EIT

Electromagnetically induced transparency is a technique used to maximize the amount of transmission of a light source through a medium. EIT is achieved by stopping the electrons in the medium from moving at the frequency of the applied light.[25] If the

electrons are not moving then they are not contributing to the dielectric constant of the medium. The electrons are stopped by driving the electrons at two sinusoidal forces of opposite phase.[26] This experiment looks at EIT using the D1 line in ^{87}Rb. First, I will discuss how the phenomenon of EIT can be looked at classically as a particle mass on a spring. Then, I will discuss the Λ configuration which is a three-state atomic system.

1. Classical Model of EIT

The classical model of EIT is a simple way to look at a much more complex phenomenon. The classical model starts just as a particle mass oscillating on a spring. Then a driving force at a specific frequency is applied to the particle mass. If the applied frequency of the driving force is a resonant frequency then the amplitude of the oscillations will continue to increase. Now, add a second identical spring to the other end of the mass. Apply the same driving force at the same resonant frequency in phase at the end of both springs and as before the amplitude of the oscillations will continually grow. If however, the driving forces at the end of each spring are applied at resonant frequency and are perfectly out of phase the amplitude will not increase. If the frequencies are perfectly out of phase, the oscillations of the springs created by the driving force will cancel each other out, leaving the particle mass motionless.

This compares excellently to an electron in an atom. First excite the atom with a laser beam set to a specific resonant frequency and the electron will begin to oscillate at that frequency. Then add a second beam with the same resonant frequency but opposite polarization. The two beams will cancel out and the electron will not oscillate. The two laser beams are labeled the signal and control fields. In EIT, the signal and

control fields cancel out and the atom is not able to absorb the light.

2. The Λ Configuration

The Λ configuration gets its name from the shape the transitions form. This configuration is a simplified version of the state of the atom. There are multiple types of EIT including V-type and ladder-type configurations, but in this experiment the lambda-type is used, which is the first type of EIT that was observed.[27] The Λ configuration consists of two lower level energy states that are coupled to the same excited state. I will label the two lower energy states as $|b\rangle$ and $|c\rangle$ and will label the excited state as $|a\rangle$. The three states each have a specific energy associated with it. The transitions between two states depend on the energy difference between the states. Exciting atoms to transition from $|b\rangle$ and $|c\rangle$ to the excited state $|a\rangle$ is done using a laser beam in this experiment. Therefore, a specific frequency of the laser beam will give the needed energy.

Rabi frequencies are used to couple the lower energy states to the excited state. The states $|b\rangle$ and $|a\rangle$ are coupled by the control field with Rabi frequency labeled Ω_C. The states $|c\rangle$ and $|a\rangle$ are coupled by the signal field with Rabi frequency Ω_S. The Rabi frequencies are defined as,

$$\Omega_C = \frac{-\wp_{ab} \cdot \mathbf{E}_c}{\hbar} \quad \text{and} \quad \Omega_S = \frac{-\wp_{ac} \cdot \mathbf{E}_S}{\hbar} \tag{24}$$

Where $\wp$'s are the electric dipole moment from $|a\rangle$ to $|b\rangle$ or $|c\rangle$ and the $\mathbf{E}$'s are the electric field vector of the control and signal fields.

The signal and control fields are applied with the laser beam. The laser is split into two separate beams and one beam is given right circular polarization, and the other is given left circular polarization.

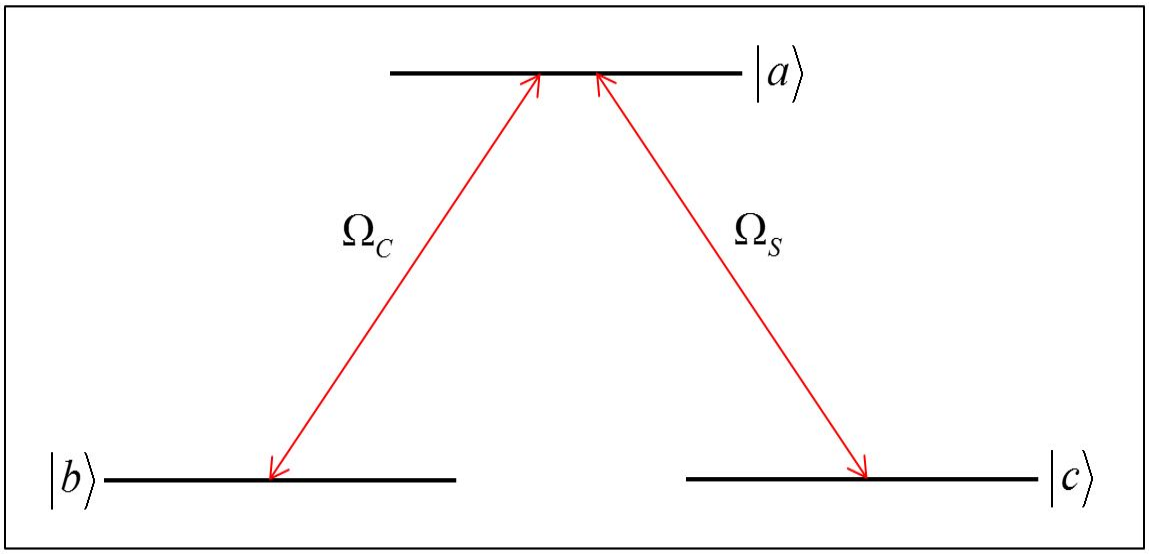

Fig. 9.[28] The Λ configuration. States $|b\rangle$ and $|c\rangle$ are degenerate and state $|a\rangle$ which is excited. The Rabi frequencies couple $|b\rangle$ and $|c\rangle$ to $|a\rangle$. Quantum interference occurs when the states are driven at the Rabi frequencies at the same time. The quantum interference cancels the absorption and the transmission increases.

So-called bright and dark states can be made by creating a linear combination of states $|b\rangle$ and $|c\rangle$. The bright state is labeled as $|B\rangle$ and the dark state is labeled as $|D\rangle$. The new system of three states $|B\rangle$, $|D\rangle$, and $|a\rangle$ are all mutually orthogonal. The states $|b\rangle$ and $|c\rangle$ are combined such that the bright state allows transitions up to state $|a\rangle$, but the dark state does not allow transitions up to state $|a\rangle$. Atoms in state $|a\rangle$ have the same probability of decaying down to the bright or dark state. With this configuration and enough time all atoms will eventually be in the dark state. After all atoms are in the dark state no more absorption occurs and all the light will be

transmitted through the atoms.

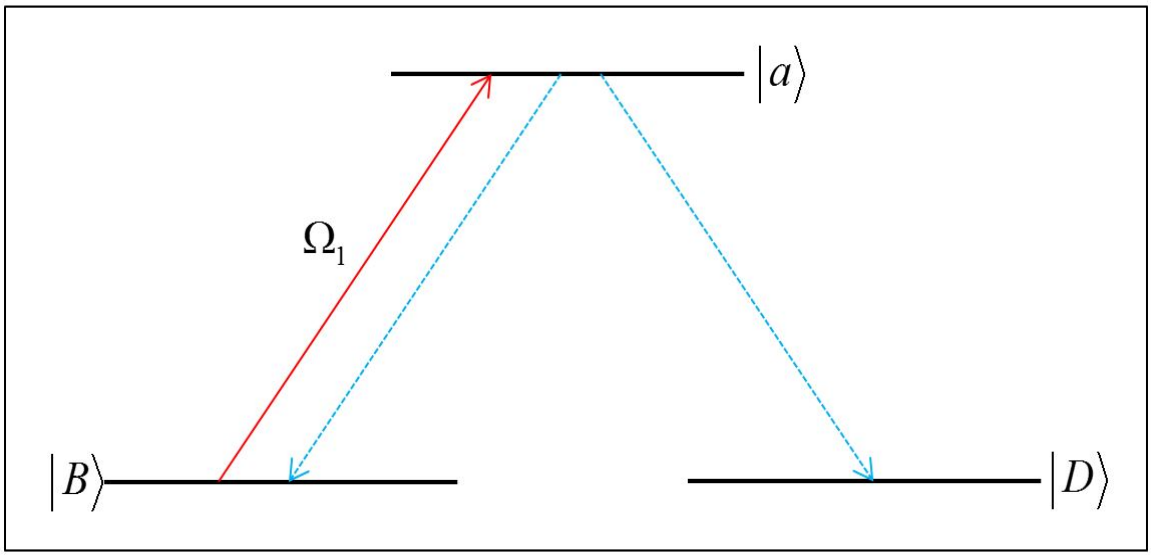

FIG. 10.[29] The system of the state $|a\rangle$, the bright state $|B\rangle$, and the dark state $|D\rangle$. The blue lines represent spontaneous emission down to lower levels. The bright state allows transitions to $|a\rangle$ where Ω_1, labeled by the red line, couples states $|B\rangle$and $|a\rangle$. The dark state does not allow transitions to $|a\rangle$. The atoms decay from $|a\rangle$to $|B\rangle$and $|D\rangle$with equal probability. Eventually, all atoms will be in the dark state.

III. Experimental Apparatus

No experiment can be done without equipment. In this section I will discuss the equipment and setup I used throughout the experiment. Figure 11 is the overhead picture of the experimental layout and FIG. 12 is the schematic diagram. The components of the apparatus were put together many years ago and have been used in many other theses. The main change made this year to the experimental layout was moving the interaction arm to the top of the setup, which allowed for one less mirror to be used. This was done because horizontally and vertically polarized light reflects differently off a mirror. Removing the mirror improves the quality of the polarization.

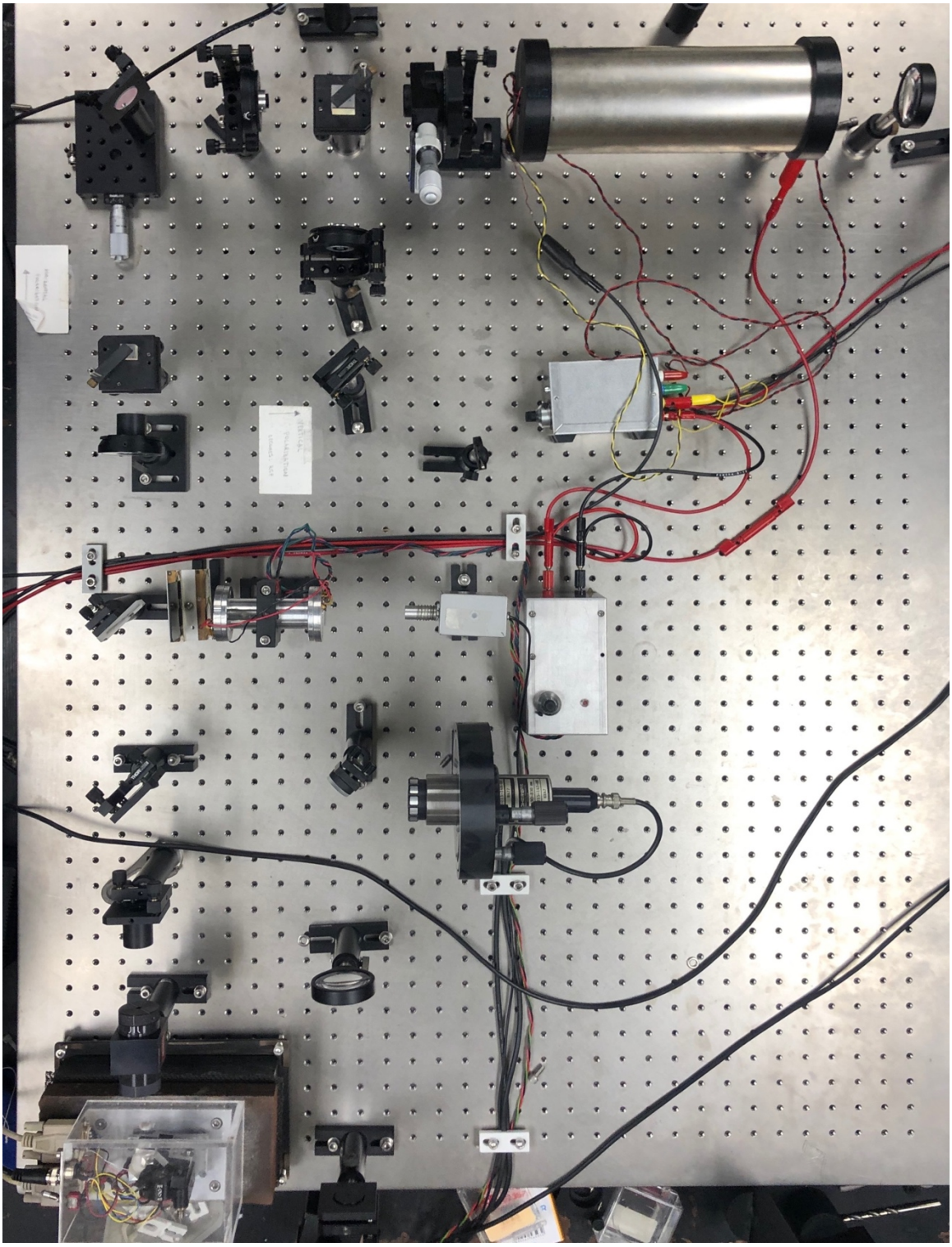

FIG 11. Overhead picture of the Experimental apparatus

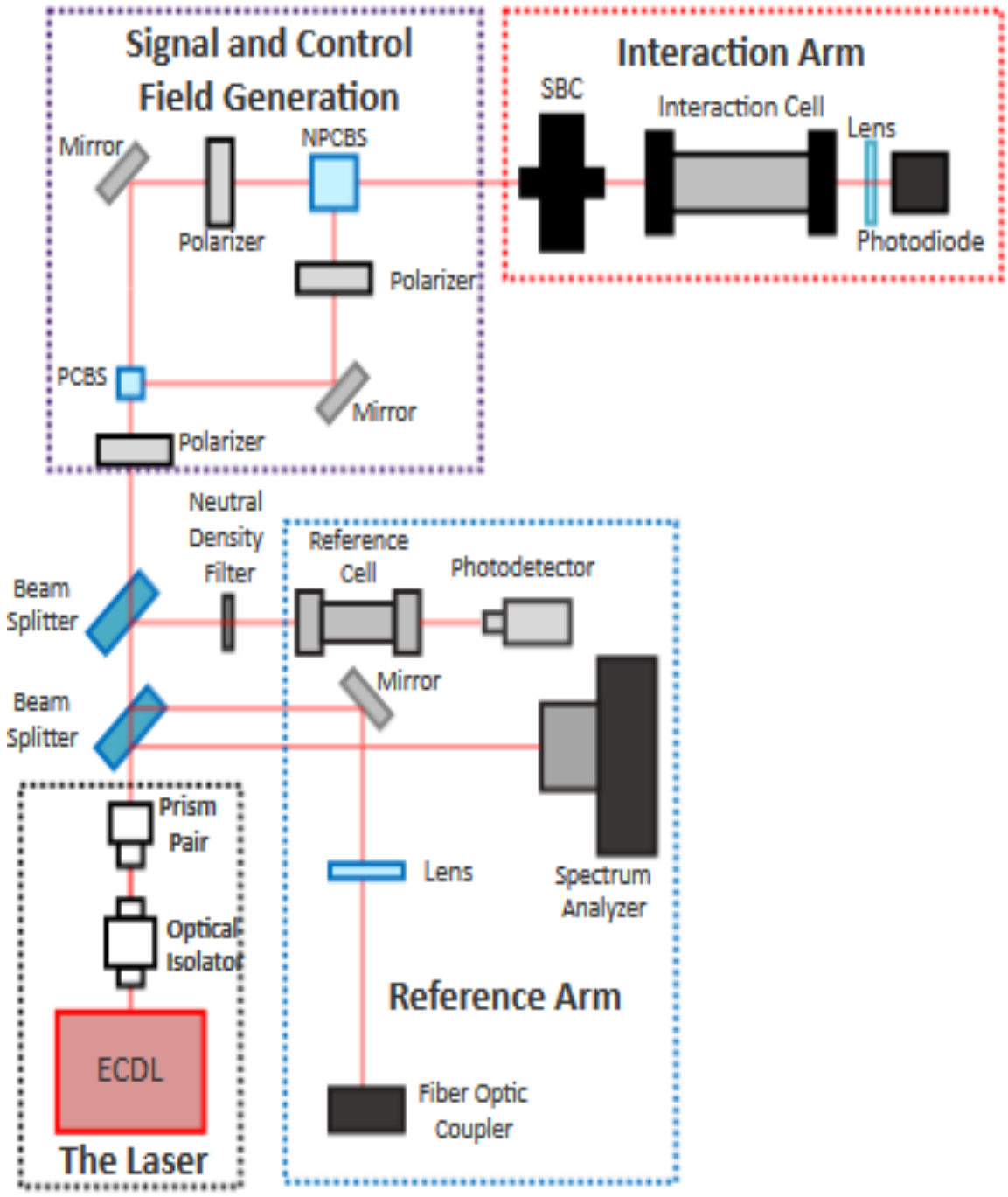

FIG 12: Schematic diagram of the experimental setup.

Four different sections of the apparatus are shown in the schematic: the laser, the reference arm, the signal and control field generation, and the interaction arm.

The experiment starts in the laser section which consists of the external cavity diode laser (ECDL), optical isolator, and the prism pair. The purpose of this section is to produce the only laser beam that will be used throughout the experiment. The next section of the experimental apparatus is the reference arm. The reference arm contains the reference cell, a photodetector, a spectrum analyzer, and the fiber optic coupler. The purpose of this section is to help us orient the laser in the way we will need it for the rest of the experiment. This section is used to observe the characteristics of the laser beam and make adjustments if needed. The next section is the signal and control field generation. This section contains multiple linear polarizers, two mirrors, a polarizing cube beam splitter (PCBS), and a non-polarizing cube beam splitter (NCPBS). This section splits up the laser beam into two separate beams, then one beam is made to have vertical linear polarization and the other is made to have horizontal linear polarization. The beams are then combined and made to be right on top of one another. The final section is the interaction arm. This section contains a Soleil-Babinet Compensator (SBC), the interaction cell, a lens and a photodiode. In the interaction cell in his section is where the EIT will occur. Lastly, I will discuss the electronic instrumentation used and the many connections made between devices.

A. The Laser

The Laser section of this experiment creates a circular steady beam that can be easily controlled. The first component of this section is the external cavity diode laser (ECDL). The ECDL used is a tunable single-mode diode laser that emits an infrared laser beam at 795 nm. The ECDL works using a laser diode chip, a diffraction grating, and a

mirror. The laser works by sending the first-order diffracted beam from the grating back into the laser diode chip. At the same time, the zeroth order light reflects off and forms the output laser beam. The first-order beam into the laser diode chip creates a standing wave between the diode and the grating.[30]

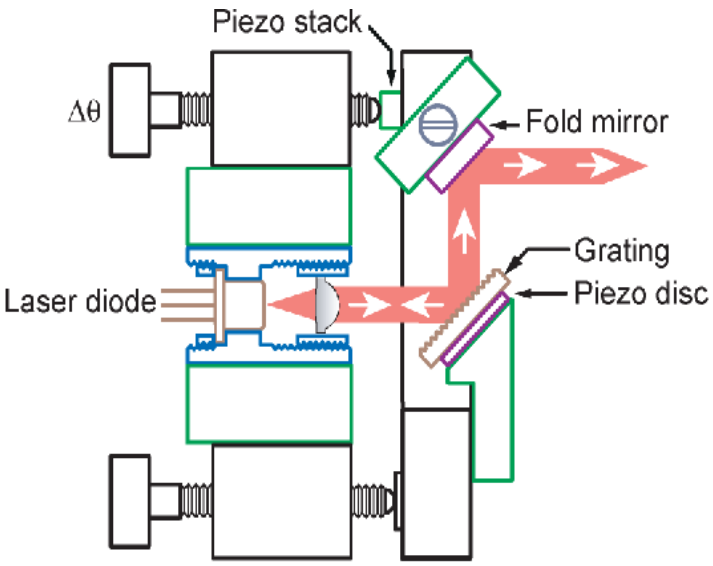

FIG 13.[31] Inside the ECDL. The first and 0th order diffraction create an output laser beam. A standing wave is created between the Laser diode and the grating

Next, the laser beam enters the optical isolator. The optical isolator only allows light to go through in one direction. This prevents optical feedback which can interfere with the laser. Optical feedback can disturb the standing wave created between the laser diode chip and the grating. The last piece of the laser section is the anamorphic prism pair. The prism pair creates a more circular beam shape. This is needed because the ECDL creates a laser beam with an elliptical beam shape. The anamorphic prism pair gives a more symmetrical beam which is easier to work with in this experiment. Having a

symmetrical beam is a benefit because the alignment of the beam is extremely important. In the signal and control field generation portion of the experiment, the beam will be spilt up then realigned back on top of itself. Having a circular and symmetrical beam shape makes the alignment much easier.

B. Reference Arm

The reference arm portion of the apparatus contains a reference cell, a photodetector, a spectrum analyzer, and a fiber optic coupler. Two beam splitters sent some light from the laser beam into the reference arm. The first beam splitter reflected light at the front and back of it into the reference arm. The first reflection then hit the mirror and went into the fiber optic coupler. The fiber optic couple connected to a wavemeter using a fiber optic cable, and the wavemeter gave the approximate wavelength of the light. The light that reflected off the back of the beam splitter went into the spectrum analyzer. The spectrum analyzer used was a Coherent Components Group Model 240 spectrum analyzer which was used to observe small frequency changes of the laser.

A portion of the light that passed through the first beam splitter hit the second beam splitter and reflected into the reference cell in the reference arm. The light passed through the reference cell and into the photodetector which measured the transmission of light through the reference cell. The reference cell contained ^{87}Rb and ^{85}Rb, whereas in the interaction cell, where we will observe EIT, there is only the ^{87}Rb isotope. The light passed through the reference cell and into the photodetector, which connected to an

oscilloscope, which displayed the transmission spectrum. An example of the absorption spectrum from the reference cell is displayed in FIG. 14. The reference arm made it possible to put the laser in the right state for the rest of the experiment to work.

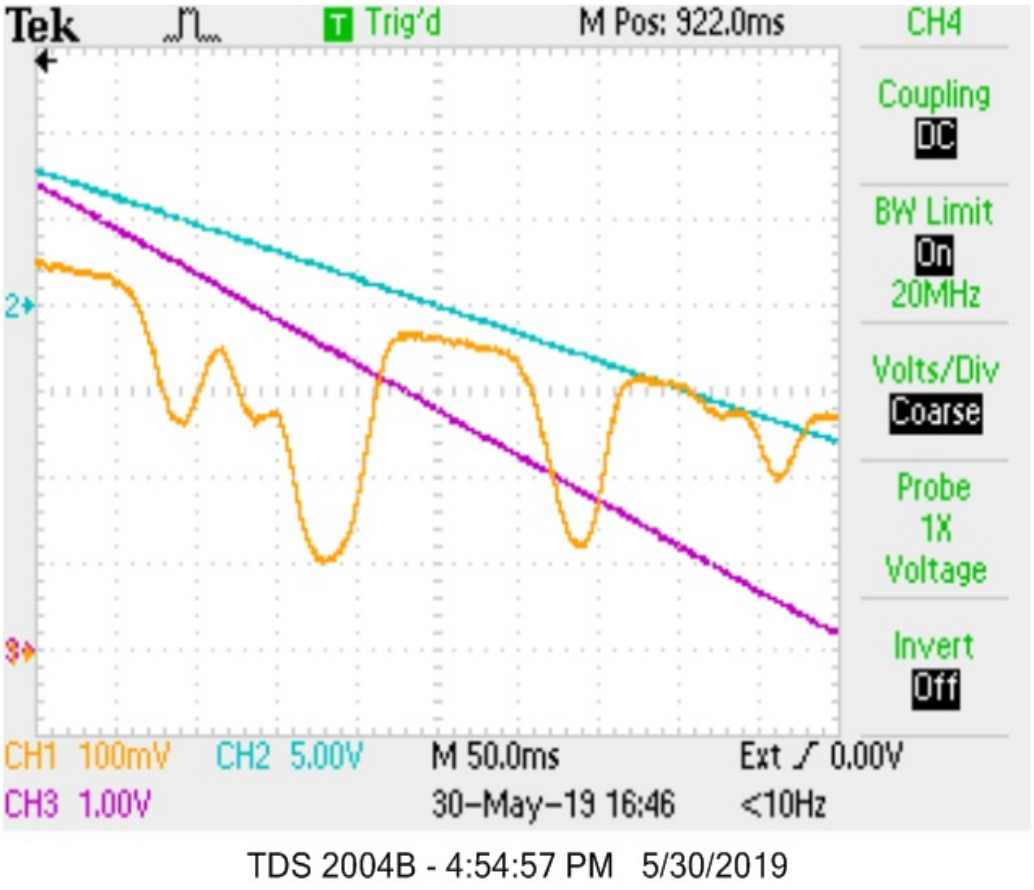

FIG 14. Screenshot of the oscilloscope displaying the absorption spectrum in the reference cell. This scan contains the D1 line of ^{87}Rb and the D2 line of ^{85}Rb. Here channel 1 is the transmission through the reference measured by the photodetector.

C. Signal and Control Field Generation

The signal and control field generation contained three Glan-Thompson linear polarizers, a polarizing cube beam splitter (PCBS), two mirrors, and a non-polarizing cube beam splitter (NPCBS). The laser beam first went through one of the polarizers to

ensure that the laser was polarized at a 45° angle above the horizontal. Next, the laser hit the PCBS. The PCBS split the incident light into two separate beams as shown in FIG. 15. The beam reflected to the right became vertically polarized and the beam transmitted through the PCBS became horizontally polarized. Next, both beams encounter a mirror which reflected them both in the direction of the

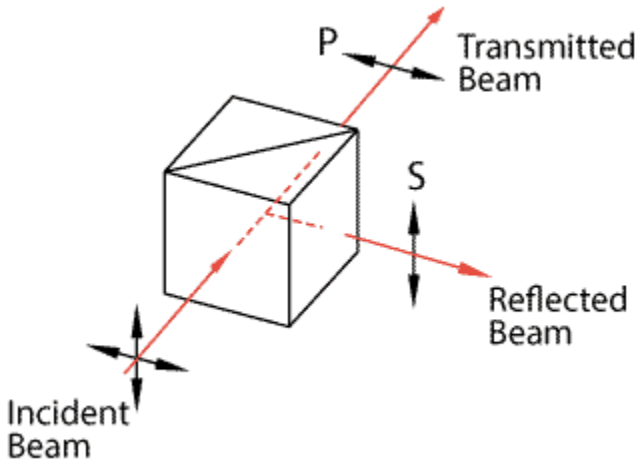

FIG. 15.[32] The Polarizing Cube Beam Splitter. The PCBS split the incident beam into a reflected beam that was vertically polarized and a transmitted beam that was horizontally polarized.

NPCBS. Before reaching the non-polarizing cube beam splitter, the two beams each encountered another polarizer. The polarizer for the vertical beam was set to 90° above the horizontal and the polarizer for the horizontal beam was set for 0° above the horizontal. This ensures the two beams will be vertically and horizontally polarized and will be orthogonal to each other. The beams then both reached the NPCBS. The NPCBS recombined the beams so they were coincident, without affecting the polarization of either beam. Aligning the beams was a difficult and important part of the experiment

and will be discussed more in a later section. After the beam left the reference arm, it was really two separate beams, one vertically polarized and one horizontally polarized, that are right on top of one another.

D. Interaction Arm

The interaction arm was the final point in our experiment and is where the EIT took place. The interaction arm contained a Soleil-Babinet Compensator (SBC), an interaction cell, a lens, and a photodiode. The laser bean first went through the SBC. The SBC changed the vertically and horizontally polarized light to right and left circularly polarized light. The right- and left-circularly polarized light then entered the interaction chamber. The interaction chamber had two layers of magnetic shielding to block unwanted magnetic fields. The interaction chamber contained a solenoid which created a magnetic field for the experiment. Inside the interaction chamber was the heated ^{87}RB cell (pictured below) with 5-torr He buffer gas. The buffer gas was an addition made a few years ago to improve the quality of EIT. The buffer gas improved the quality of EIT by restricting the motion of the rubidium atoms and decreasing the amount of collisions with the cell walls. The laser beam then left the rubidium cell and was focused onto the photodiode. The photodiode allowed us to measure the transmission through the cell, and permitted us to observe EIT.

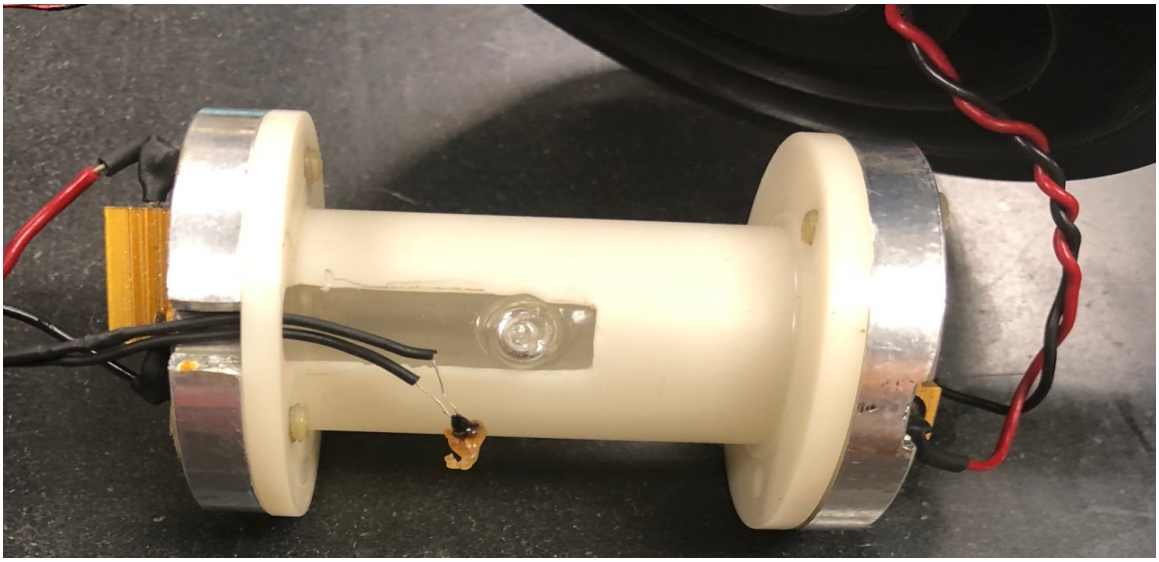

FIG 16. Heated ^{87}Rb with buffer gas cell while it was removed from the magnetic shielding of the interaction chamber. Resistors on the sides were heated to heat up the entire cell to the desired temperature. Here, the thermistor is not attached to the Rb cell.

E. Electronic Equipment

The electronic equipment furnished power to the components and monitored the status of the experiment. In this experiment a wide variety of equipment was used: multiple digital oscilloscopes, a DC power supply, a temperature controller, a laser diode controller, three function generators, a so-called control box, a wavemeter, a digital multimeter, a power meter, and a power supply box.

Getting the laser to properly run required multiple different instruments. The ThorLabs Temperature Controller TEC 2000, ThorLabs Laser Diode Controller LDC 500. Many adjustments were made simultaneously to get the laser working properly at the right frequency. The temperature controller measured and controlled the temperature of the laser. This was accomplished by a thermistor mounted adjacent to the laser. A thermistor is a resistor whose resistance has a heavy dependence on temperature. The

laser diode controller measured and controlled the current going into the laser diode chip. The control box controlled the angle of the grating and also controlled the current going into the laser diode chip. The Burleigh Wavemeter jr. was used early in the experiment to get the laser to the right approximate wavelength. A Stanford Research Systems Function Generator Model DS345 controlled the frequency at which the laser scanned. The frequency was usually set to 0.1 Hz, but was occasionally increased or decreased help tune the laser. The Tektronix TDS 220 oscilloscope also was used to help set the laser. This oscilloscope connected to the spectrum analyzer and displayed the frequency of the laser. This was crucial to getting the laser to work properly. Watching the laser scan on the oscilloscope was the best way to determine how well the laser was working and was necessary to improve the quality of the laser. The Tektronix TDS 2004B Oscilloscope also was used to look at the performance of the laser. This oscilloscope connected to the photodetector, which measured the transmission through the reference cell, FIG. 14, was taken from this oscilloscope. This oscilloscope was also used while working to achieve EIT as well. We used the output from the photodetector to set the laser at the frequency that would give the exact transmission needed for EIT.

Most of the remaining equipment used helped make EIT possible. The Agilent E3611A DC Power Supply was used to heat the reference cell and the interaction cell. This was needed to put the rubidium atoms in a vapor phase. The Fluke 45 Dual Display Multimeter was used to measure the voltage across and current going to a thermistor on the interaction cell. Using the Fluke 45 multimeter and a LabView program, I created a graph that related the temperature of the interaction cell to the time it was being

heated (FIG 17). We used a Pasco Scientific Digital Function Generator to control the magnetic field in the solenoid in the interaction chamber. Another piece of equipment used was the ThorLabs PM100D Power Meter. This was used in many different parts throughout the experiment. The power meter combined with a LabView programmed helped create better polarization both linear and circular. The power meter was also used to measure the power of both the horizontally and vertically polarized beams and ensure they were equal.

FIG. 17. Temperature of the interaction cell vs. Time graph. This was created to see how long it takes to heat the interaction cell to the temperature needed for EIT. The data taken for this was taken using the Fluke 45 and a LabView program that simultaneously recorded time, the voltage across the thermistor on the interaction cell, and the current into the resistor.

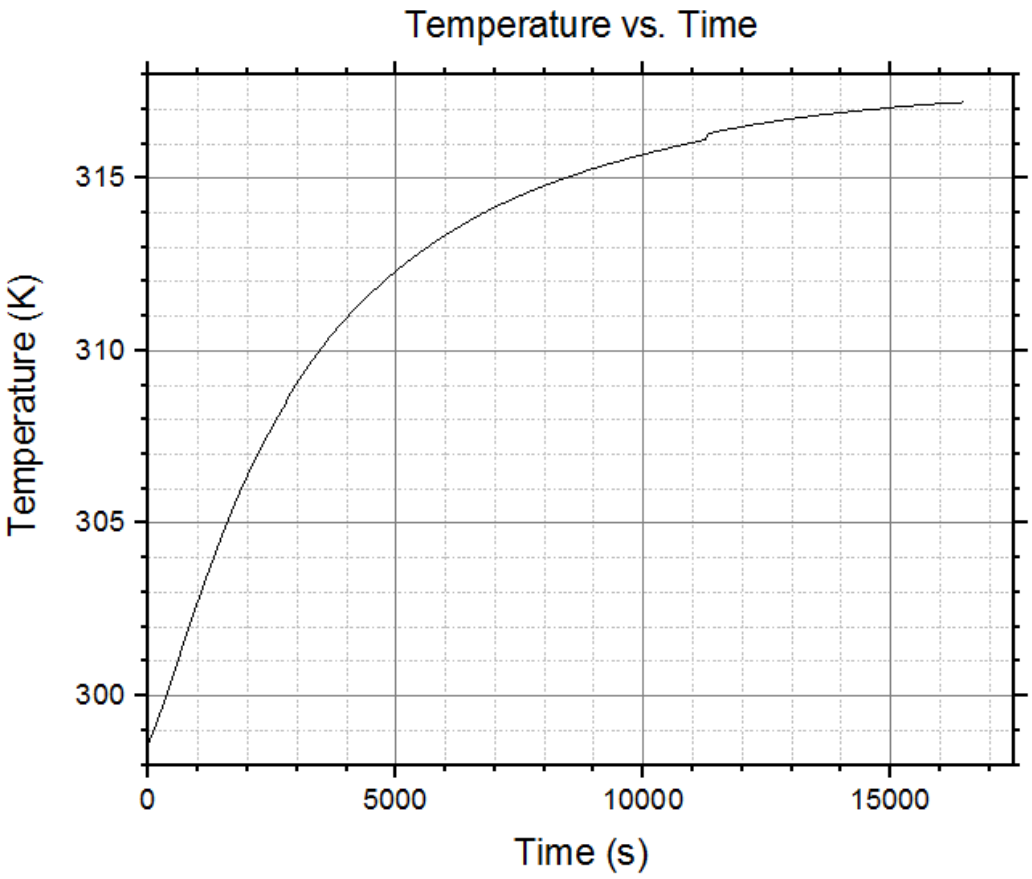

IV. Experimental Data

The goal of the experiment was to achieve the best EIT possible. I theorized that an important factor in the quality of EIT was the quality of the circular polarization. To achieve the best quality circular polarization, I would also need the best quality linear polarization. I spent a lot of time in the lab making small adjustments in alignment and technique to achieve higher quality polarization than students had in past theses at Lake Forest College.

A. Polarization

I spent the vast majority of my time in the lab running trials and taking data trying to achieve the highest quality polarization. I adjusted equipment, changed the layout of the setup, and made sure everything was level. While working on the linear polarization, I worked to make sure both beams were exactly perpendicular in their polarization, reached the same maximum power transmitted when the analyzer polarizer was turned 180°, and achieve the best extinction in each beam. For circular polarization, I worked to minimize the effect of the angle of the analyzer polarizer on the power transmitted.

1. Linear Polarization

High quality linear polarization is important in this experiment because high quality circular polarization cannot be achieved without good linear polarization. A very important piece of equipment I used for improving the quality of both linear and circular

polarization was used with the analyzer polarizer. The analyzer polarizer is the second polarizer in a set of two polarizers. It is called the analyzer because when the first is left unchanged, changing the second polarizer and measuring the power transmitted through will show how the first polarizer is working. For the analyzer polarizer in this set up, I used a polarizer connected to a gear that rotated the polarizer by 1.8° at a time. This was connected to a LabView program that would

FIG. 18. Analyzer polarizer on rotation station. The polarizer (on the left) would

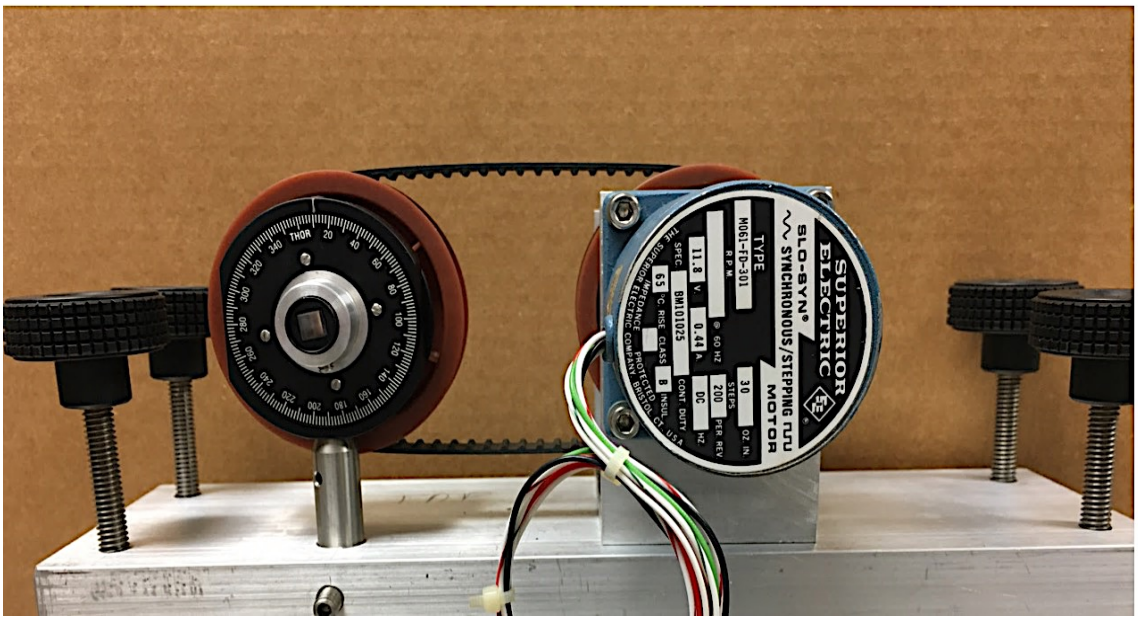

be turned by the gear (on the right). The gear could be turned by a LabView program or manually. Either way the gear was turned the polarizer would move 1.8° at a time.

move the polarizer 1.8° and record the power transmitted through the polarizer measured by a power meter. I placed the analyzer polarizer after the Signal and Control Field Generation section of the setup and placed the power meter behind it. For the data taken, the LabView program was set to take 400 data points. Taking 400 data points would rotate the analyzer polarizer 360° around twice. I chose to rotate the polarizer completely around twice to ensure that the data was consistent. I used this

contraption to improve the quality of linear polarization in 3 different ways. First, I ensured that the polarization of the two beams were in fact perpendicular to each other. Second, I adjusted the mirrors and polarizers until the beams reached the same power at points where the angle of the analyzer polarizer was shifted 180°. Lastly, I attempted to maximize the extinction of each beam, meaning that the minimum power transmitted through the analyzer polarizer at a certain angle would be as close to 0 as possible.

a. Perpendicular Polarizations

The first use of this contraption was to determine if the linear polarization of the two separate beams after being split by the PCBS were perpendicular. To determine how perpendicular the beams were, I measured the power transmitted through the analyzer polarizer by each beam separately. After that, I graphed the power transmitted vs. the angle of the analyzer polarizer for each beam on the same graph.

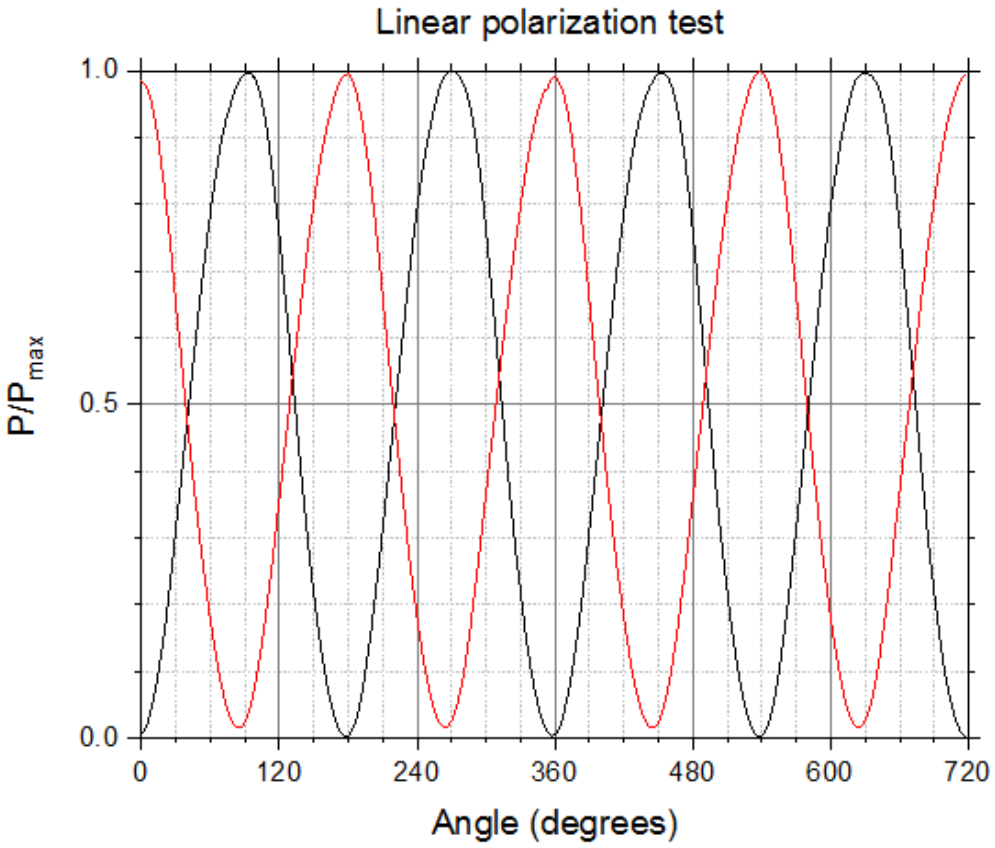

FIG. 19. Graph of the amount of power transmitted for each beam at different angles of the analyzer polarizer. The red line is from the vertically polarized beam and the black line is from the horizontally polarized beam.

This graph can be used to see if the polarization of the beams is perpendicular by seeing where the different lines intersect. If the beams were perpendicular, the lines would intersect every 90° exactly on the 0.5 horizontal line. Looking at the graph in FIG 19, the lines clearly are not intersecting on the 0.5 horizontal line. I fixed this by adjusting one of the initial polarizers for one of the beams and retaking data to see if it improved how perpendicular the polarization was. I repeated this until the polarization of the beams looked perfectly perpendicular by eye. Next I used Malus' Law[33]

$$I = I_0 \cos^2 \theta \tag{25}$$

From this we see the power transmitted is proportional to the square of the angle between the polarized light and the angle of the polarizer. Using this fact, I fit curves to the graphs of percent of power transmitted through the polarizer vs. angle of the polarizer. Doing this I could calculate the angle between the polarizations of the two beams and make further adjustments.

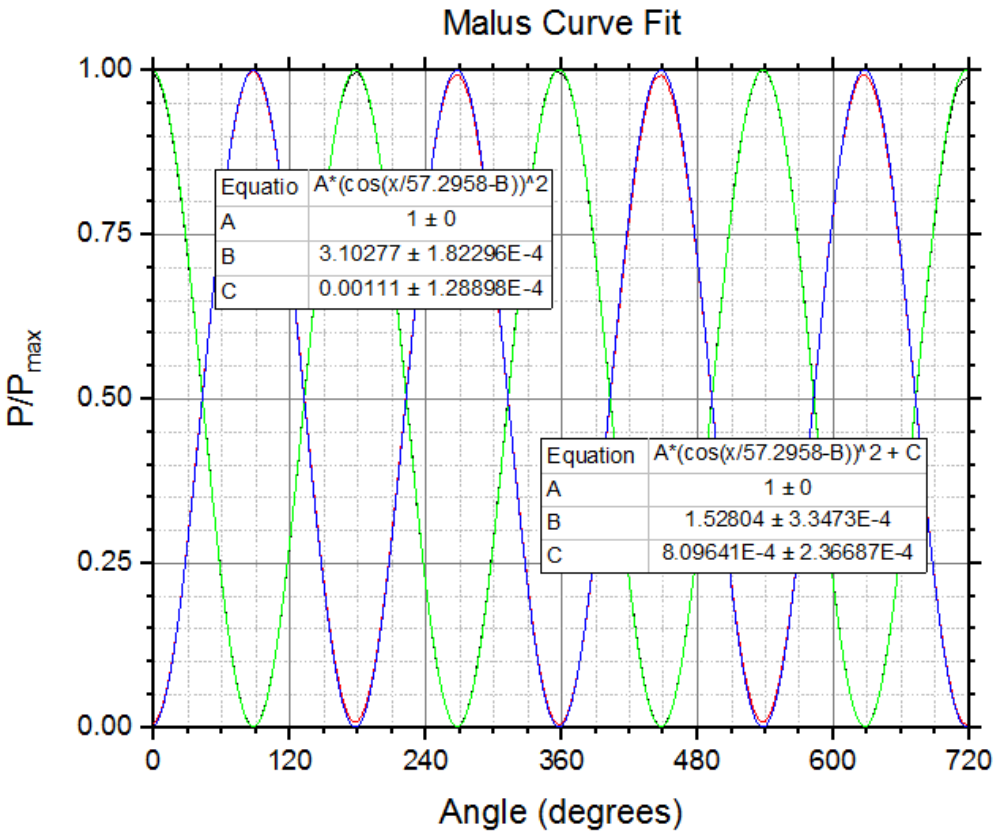

FIG. 20. Malus' Law curve fit of the power transmitted through the analyzer polarizer vs. the angle of the analyzer polarizer. The green curve fit represents the vertically polarized beam and corresponds with the box in the upper left, and the blue curve fit represents the horizontally polarized beam.

From the graph above the angle between the polarizations of the two beams can be determined from the B values. The B values represent the offset of the curve from the origin in radians. Converting from radians to degrees, the vertically polarized beam is offset by 177.8° and the horizontally polarized beam is offset by 88.6°. This shows the

beams are very nearly perpendicular and the angle between the polarizations is 90.2°.

b. Equal Power Transmission

The next step in improving the quality of the linear polarization was equalizer the power transmitted through the analyzer polarizer at points 180° apart. To do this, I looked at the maximum values of the power transmitted at 180° apart to see if they peaked at the same point.

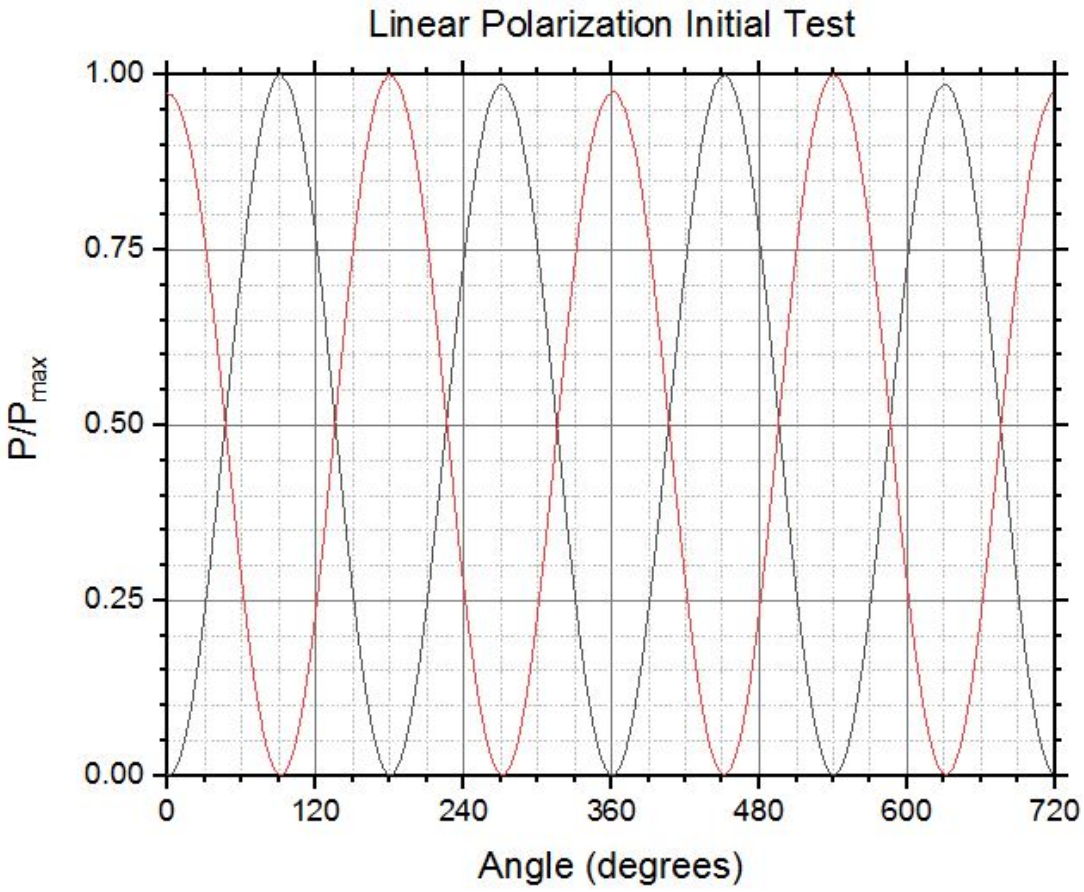

FIG. 21. Initial test to see if power transmitted through the analyzer polarizer maximized to the same value when the polarizer is turned 180°. The red line represents the vertically polarized beam, the black line represents the horizontally polarized beam.

For the initial test, both vertically and horizontally polarized beams did not reach the same peak when the analyzer polarizer was turned. I improved this by adjusting the angles of the mirrors and polarizers by small amounts then retaking data to see if there was any improvement. Repeating these adjustments and taking more sets of data I was able to improve the consistency of the peak values.

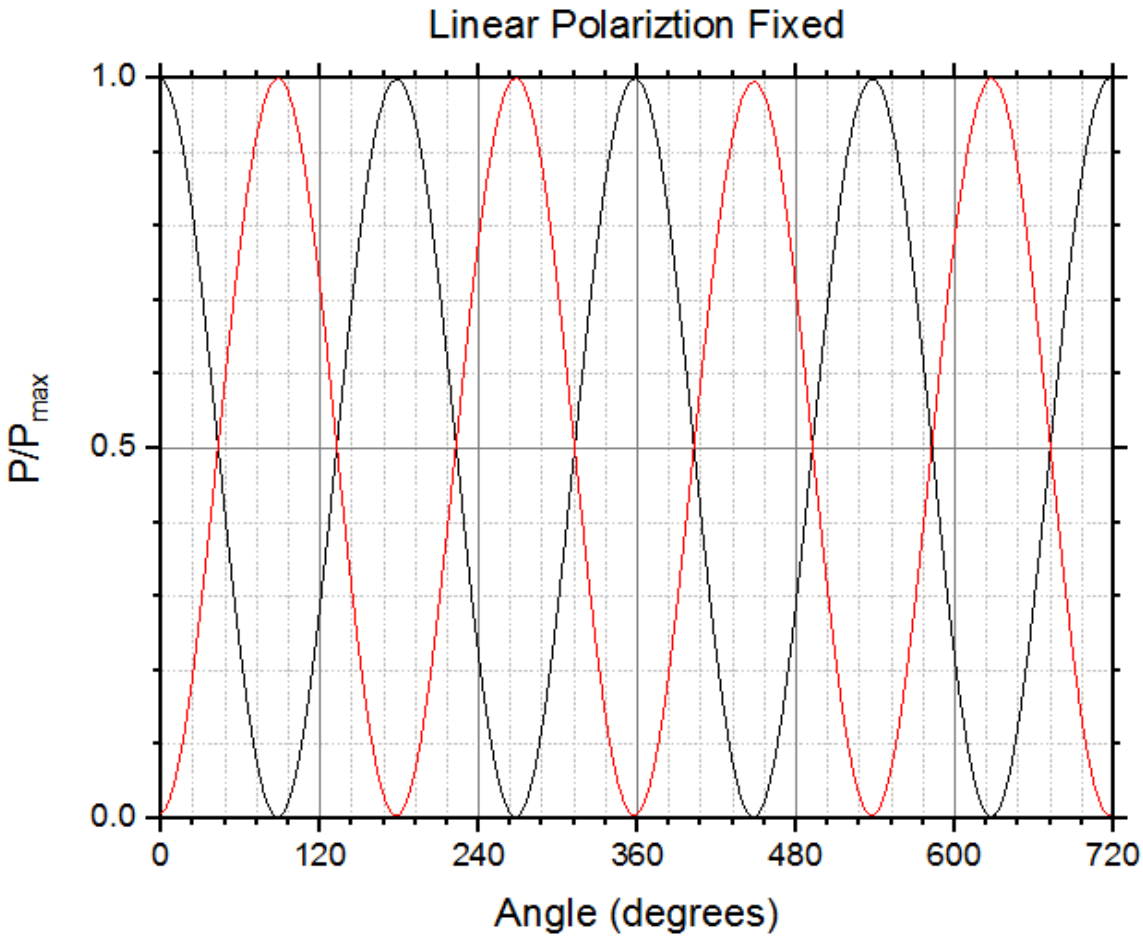

FIG. 22. Graph of the linear polarization after adjustments were made. The black line represents vertically polarized light and the red line represents horizontally polarized light.

In this graph, the peaks are much more consistent. There is one peak for the horizontally polarized light that does not reach the same power as the other peak. One peak being lower is not a big concern because when the analyzer polarizer was at the

same angle 360° away it reached the same point as the other peaks. This led me to believe that the lower value did not come from the analyzer angle, but from an inconsistency in the laser.

c. Extinction of the Beams

The final area of improvement in the linear polarization I worked on was maximizing the extinction in each beam. To maximize the extinction I attempted to get the lowest values of power transmitted through the analyzer polarizer as close to 0 as possible. Looking at graphs formatted similarly to what I have been using to improve my linear polarization so far did not work. I needed to zoom in on the lower end of the graphs to see how close they got to 100% extinction, or 0% transmission.

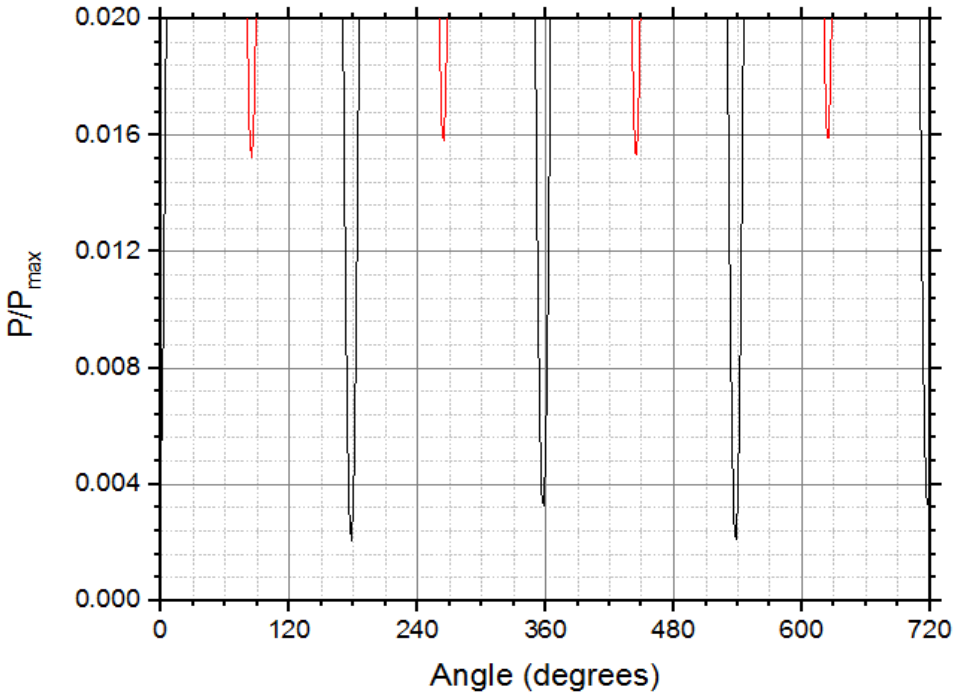

FIG. 23. Initial graph for the extinction of the linear polarization. The red dips represent the vertically polarized light and the black dips represent the horizontally polarized light. Graph is scaled on the Y axis. The graph shows from 0% transmission to 2% transmission.

The initial data shows that the vertically polarized light was only reaching about 98.4% extinction, and the horizontally polarized light was reaching 99.5% extinction. To improve this, I realigned the two beams after leaving the NPCBS. I wanted to make sure that both beams were hitting the same spot on the polarizer and coming in at the same angle. To do this, I took out the analyzer polarizer, the power meter, and the Interaction arm of the setup. I did this so I had more distance for the beams to spread out if they were not directly on top of each other. I then bounced the beams off a couple of mirrors to maximize the distance.

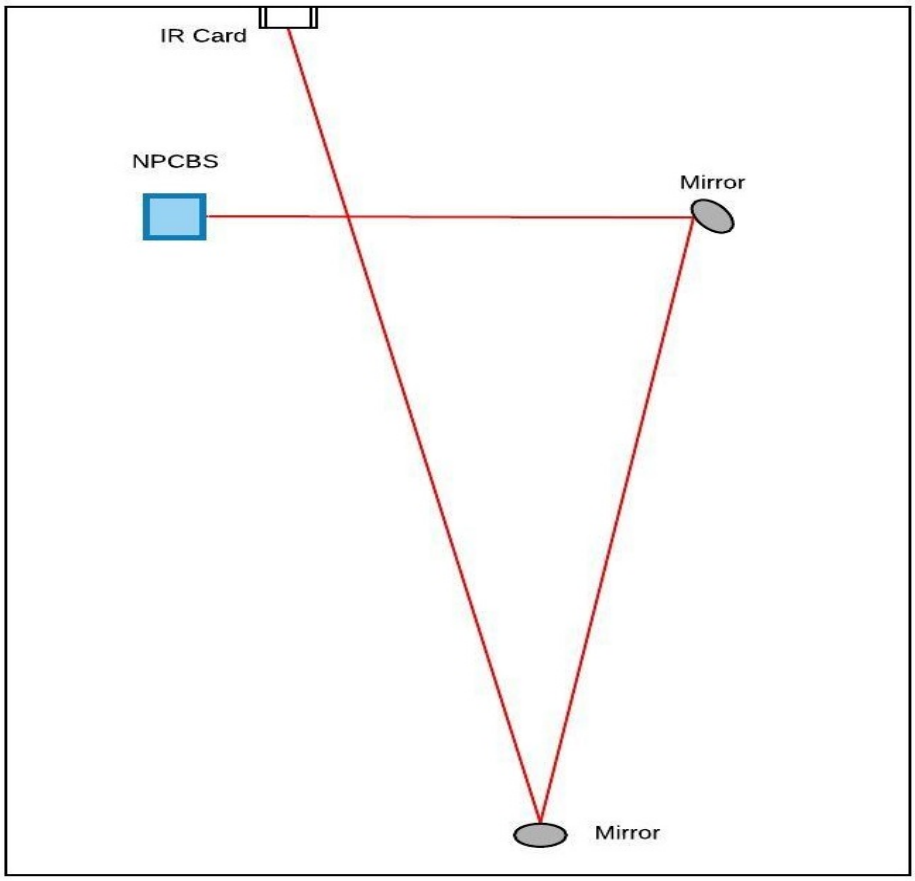

FIG. 24. Diagram of setup used to align the two beams. The rectangular box represents the lab room I was in. The red line represents the two beams on top of each other. I bounced the two beams off two mirrors and into an Infrared (IR) card that allowed me to see where the two beams hit.

To align the beams, I would use an IR card to track them as far as I could until the beams hit a wall or split too much to see on one IR card. If they hit a mirror I would keep following them until they hit the next wall or split too far. If they split too far, I would leave the IR card there then adjust the NPCBS until the beams were on top of one another again. I repeated this process until I bounced the beams off two different walls and onto the back wall where I taped an IR card and aligned the beams there. I aligned them this way because the distance from the NPCBS to the analyzer polarizer was not enough to see the splitting of the beams. Bouncing the beams off walls using mirrors allowed for more distance for the beams to split. When the beams were split by a larger amount it was easier to see how they needed to be readjusted. After this process and realigning the analyzer polarizer, I was able to improve the extinction of the two beams.

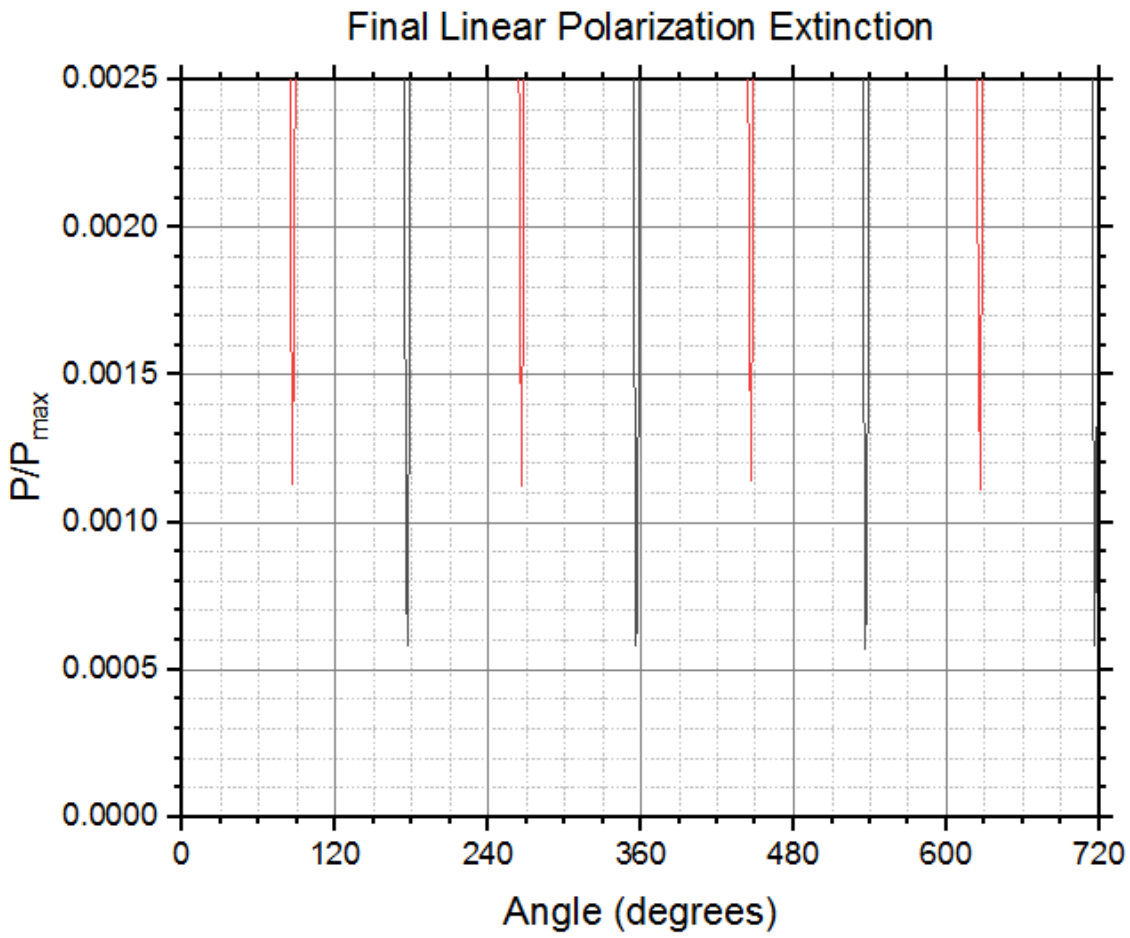

FIG. 25. Final graph of the extinction of the two beams. The red dips represent the vertically polarized light and the black dips represent the horizontally polarized light. Graph is scaled on the Y axis differently than the previous graph. The graph shows from 0% transmission to .25% transmission.

For the final set of data, the extinction of the two beams was much better. The vertically polarized beam reached almost 99.9% extinction, which is about 1/16 as much transmission as the initial test. The horizontally polarized beam reach almost 99.95% extinction, which is about 1/3 as much transmission. These improvements in linear polarization was important because it allowed for higher quality circular polarization. Maximizing the quality of the circular polarization is the next step in achieving EIT.

2. Circular Polarization

Ideally, circularly polarized light will transmit the same power through the analyzer polarizer at every angle. In this experiment, I tried to minimize the fluctuations in power transmitted for different angles of the polarizer. To obtain circularly polarized light I used a Soleil-Babinet compensator (SBS). To create circularly polarized light, I first set up two cross polarizers without the SBC. I then blocked one of the linearly polarized beams, only allowing one to go through. Then, I rotated the second, or analyzer, polarizer until the power transmitted through the second polarizer is minimized. Next, I inserted the SBC in between the crossed polarizers and rotated the SBC until the power transmitted through the analyzer polarizer was minimized again. Next, I rotated the SBC by 45°. Next, I rotated the micrometer on the SBC until the power is minimized again and set that position equal to zero. I rotated the micrometer again until another position of minimum transmission is reached. The distance shown is one wavelength of retardance. Lastly, set the micrometer to ¼ of the wavelength of retardance. This set up for the SBC gave circularly polarized light. This just needs to be done with one beam because the two beams are orthogonal. The other linearly polarized beam will become circularly polarized in the other direction.

After setting the SBC I collected data on the power transmitted through the second polarizer to check the quality of the circular polarization. Using the rotating analyzer polarizer station from FIG. 18, I recorded the power transmitted through the analyzer polarizer at different angles. To record this I had to take data for each beam separately and graph them together afterwards.

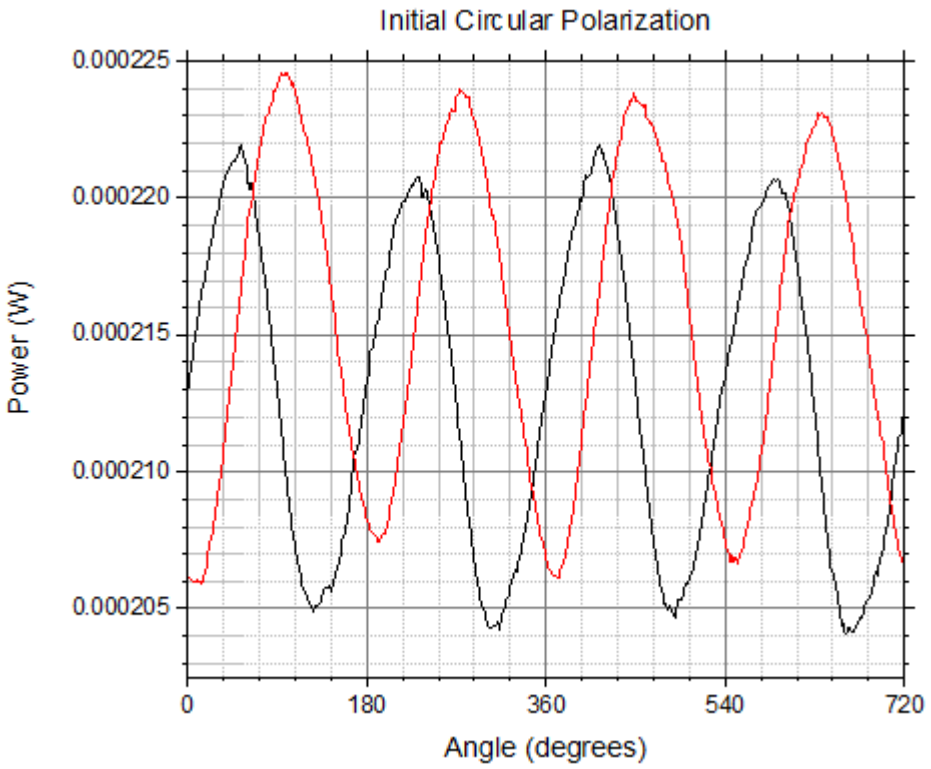

FIG. 26. Initial test for circular polarization. The red line represents the beam that was vertically polarized. The black beam represents the line that was horizontally polarized. The data represents two full rotations of the analyzer polarizer.

From the initial data set the beam that was vertically polarized fluctuated from about 206 microwatts (µW) to about 224 µW. The beam that was horizontally polarized fluctuated from about 204 µW to about 222 µW. That is a fluctuation of about ± 9 µW for each beam. The average power is about 215 µW, so the power is fluctuating by about 4.2%. To improve the quality of circular polarization the key component was

improving the linear polarization. After improving the linear polarization, I tried redoing the process to get circular polarization using the SBC. After redoing this process several times I moved onto making smaller changes. I made small adjustments to the micrometer and retook the data. If the fluctuations got smaller, I moved the micrometer a little more in the same direction. If the fluctuations grew, I adjusted the micrometer the other way. Eventually I was able to shrink the fluctuations in the data.

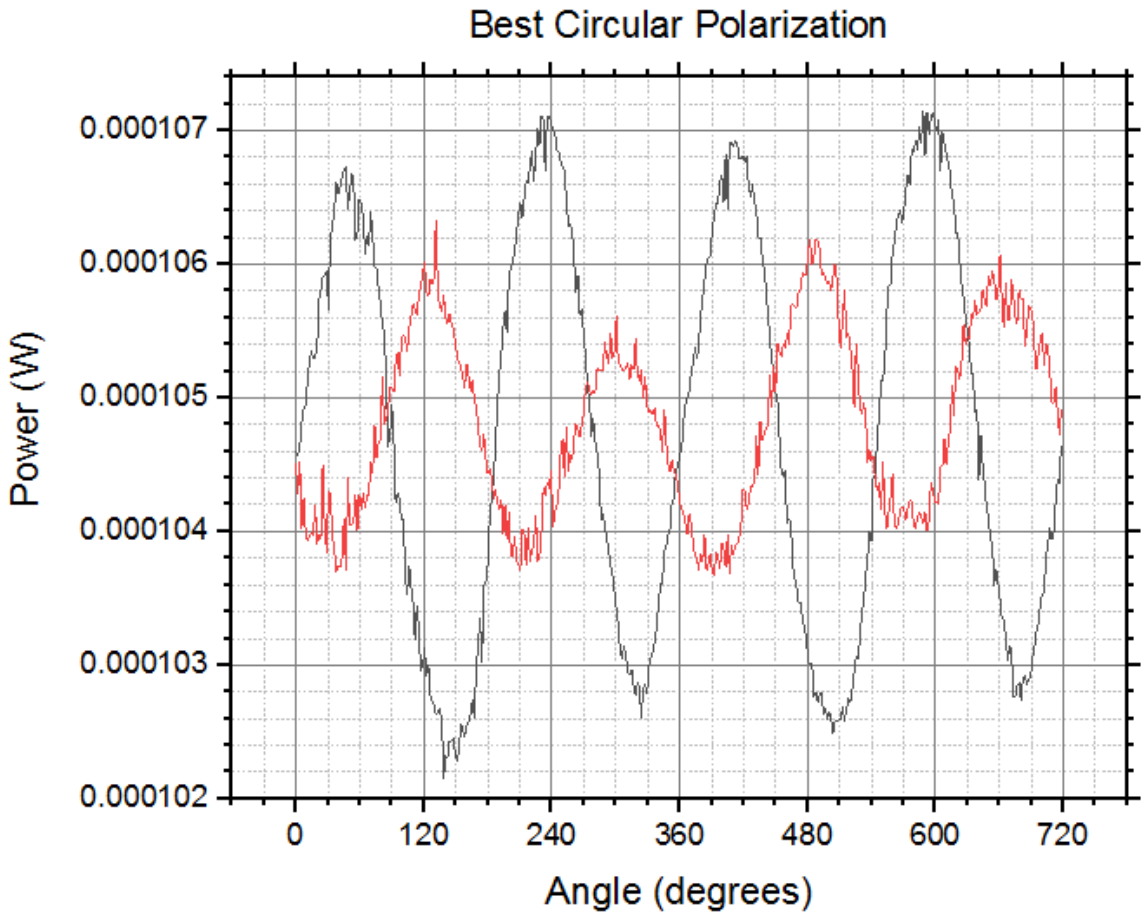

FIG. 27. Circular polarization data with minimum fluctuations. The red line represents the beam that was vertically polarized. The black line represents the beam that was horizontally polarized.

Adjusting the micrometer bit-by-bit proved to be an effective method to improve the circular polarization. Now, the beam that was vertically polarized fluctuated from

about 104 μW to about 106 μW. This is a fluctuation of about ± 1 μW, which is less than 1% of the average power. The beam that was horizontally polarized fluctuated from about 102 μW to about 107 μW. This is a fluctuation of about ± 2.5 μW, which is a little over 2% of the average power. The improvement in the circular and linear polarization will hopefully lead to improvements in EIT.

B. EIT

To achieve electromagnetically induced magnetism (EIT), I first inserted the interaction arm back in the setup and removed the analyzer polarizer. Next, I used a power supply to heat the interaction cell. I heated the cell to put the rubidium atoms in a vaporous state. I then used a function generator to sweep the magnetic field in the solenoid in the interaction chamber. I measured the transmission through the interaction cell using a photodiode. I used the lockbox to lock the frequency of the laser exactly at the frequency of the e transition in the D1 line of rubidium. When the magnetic field inside the interaction chamber was zero, EIT was observed.

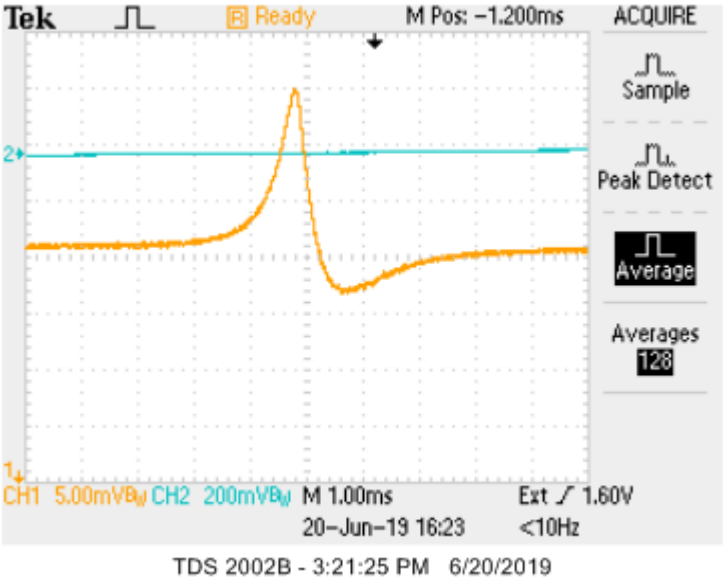

FIG. 28. The first time EIT was achieved. The blue line represents the magnetic field that was swept through the interaction chamber. The yellow line represents the transmission through the interaction cell. The horizontal lines are spaced out by 5.00 millivolts (mV). The vertical lines are spaced by 1 millisecond (ms). When the magnetic field is zero, the transmission peaks. The peak is approximately 15 mV high.

After achieving EIT for the first time, I worked to improve the quality of EIT. Better quality EIT has a more symmetric peak, has a higher peak, and has a smaller width. I adjusted the frequency and amplitude the magnetic field was sweeping through the interaction chamber to maximize the peak. I also realigned the interaction chamber so the beam went directly through center of the cell and was parallel to the chamber.

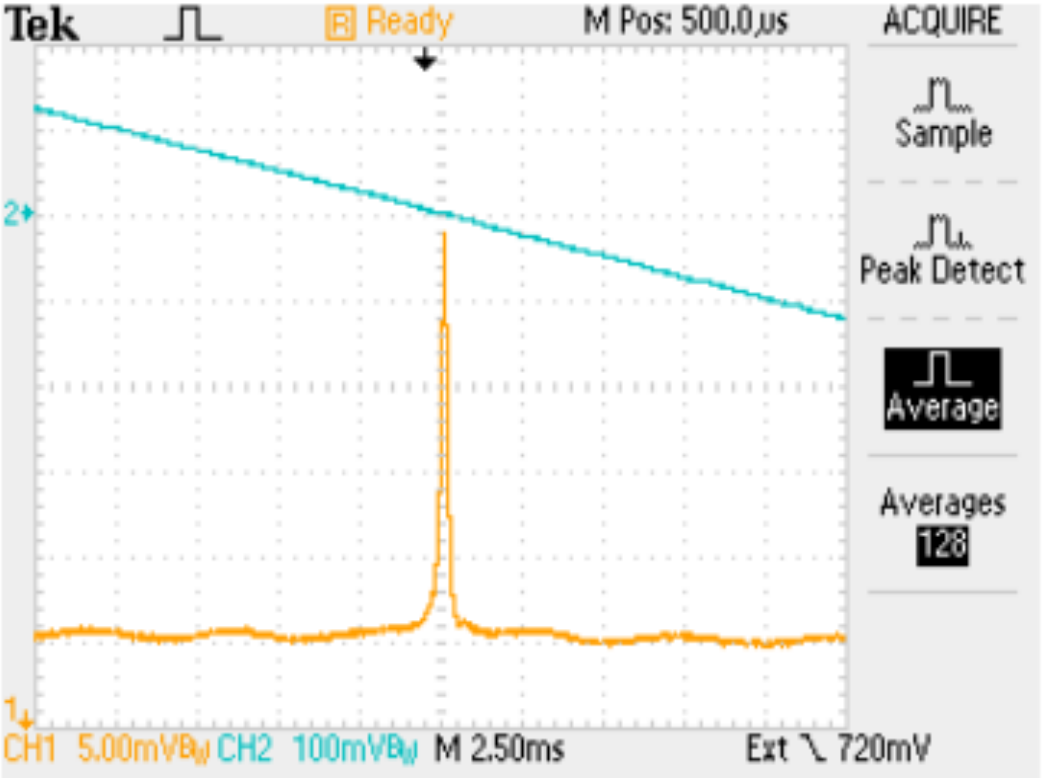

FIG. 29. This was the thinnest peak I could achieve. Here, the spacing between the vertical lines was increased to 2.5ms. The transmission was averaged out over 128 data points to reduce the noise and more clearly see the peak. The peak has a width of about 0.25 ms halfway up the peak. The peak is higher than the previous one at approximately 24 mV.

I made more small adjustments to achieve EIT with a higher peak.

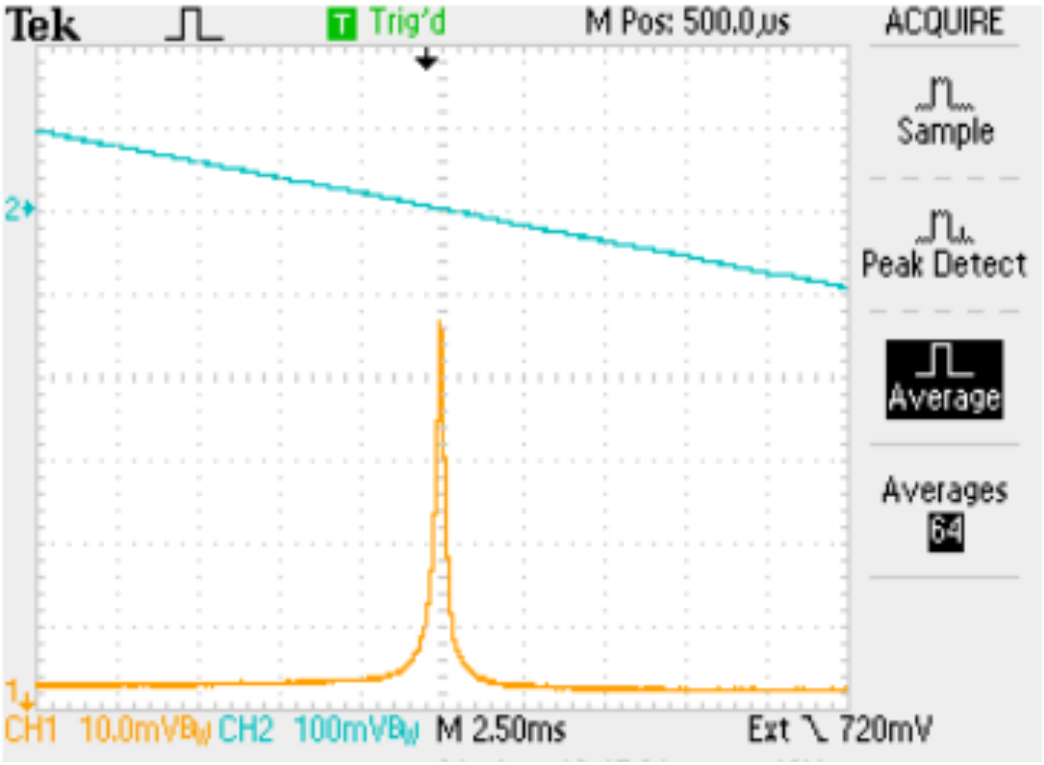

FIG. 30. This was the best quality EIT I achieved. The peak is symmetrical and is higher than the other peaks. The horizontal lines are no spaced by 10mV instead of 5mV. The peak is approximately 45 mV high.

After achieving this EIT, I would have liked to attempt to create “slow light” by inserting an acoustic optic modulator into the signal and control field generation section of the apparatus. Unfortunately, I was cut short a couple months of time in the lab due to the COVID-19 pandemic.

V. Conclusion

Electromagnetically Induced Transparency was achieved in this project. Increasing the quality of the linear polarizations allowed for higher quality circular polarizations. With better circular polarization, EIT with sharper peaks than years past was accomplished. Future experiments could focus on the effect of the quality of EIT on the quality of slow light.

REFERENCES

[1] D. J. Griffiths and D. F. Schroeter, *Introduction to Quantum Mechanics,* 3rd ed. (Cambridge University Press, Cambridge, UK, 2018) p. 131.
[2] Ibid., p. 147.
[3] Ibid., p. 155.
[4] https://en.wikipedia.org/wiki/Bohr_model (February 1, 2020).
[5] Griffiths and Schroeter, p. 297.
[6] Ibid., p. 297.
[7] Ibid., p. 302.
[8] . https://www.chegg.com/homework-help/hydrogen-fine-structure-splitting-2p-state-50-ev-percentage-chapter-36-problem-54p-solution-9780805302967-exc.
[9] M. M. Kash (private communication).
[10] Griffiths and Schroeter, p. 311.
[11] Ibid., p. 312.
[12] D. A. Speck, *Rubidium 87 D Line Data*, available online at https://steck.us/alkalidata (last revised November 21, 2019) p. 3.
[13]M. M. Kash (private communication).
[14] Speck, *Rubidium 87 D Line Data,* p. 3.
[15] Ibid., p. 3.
[16] M. A. Fortman, undergraduate thesis, Lake Forest College, 2018, p. 5.
[17] Speck, *Rubidium 87 D Line Data,* p. 5.
[18] Ibid., p. 17.
[19] Ibid., p. 27.
[20] P.Siddons, C. S. Adams, C. Ge, and I. G. Hughes*,* J. Phys. B-Atl. Mol. Opt. **41** 155004 (2008).
[21] Griffiths and Schroeter, p. 420.
[22] K. Spotts, undergraduate thesis, Lake Forest College, 2014, p. 17.
[23] D. H. Goldstein, *Polarized Light*, 3rd ed. (CRC Press, Boca Raton, FL, 2011).
[24] https://www.pinterest.com/pin/375698793897356065/.
[25] S. E. Harris, Phys. Today, **50**, 36 (1997).
[26] Ibid., p. 36.
[27] A. J. Olsen and S. K. Mayer*,* Am. J. Phys. **77** 116 (2009).
[28] Fortman, p. 9.
[29] Ibid., p. 10.
[30] C. Ye, *Tunable External Cavity Diode Lasers* (World Scientific Publishing, Hackensack, NJ, 2004) .
[31]S. D. Saliba, M. Junker, L. D. Turner, and R. E. Scholten, Appl. Opt. **48** 6692 (2009).
[32] http://rmico.com/polarizing-cube-beamsplitters.
[33] F. L. Pedrotti, L. M. Pedrotti, and L. S. Pedrotti, *Introduction to Optics,* 3rd ed. (Cambridge University Press, Cambridge, UK, 2018) p. 351.